Theoretical Study of the Fragmentation Pathways of Norbornane in Its Doubly Ionized Ground State

Stefan Knippenberg, Balázs Hajgató, Jean-Pierre François, and Michael S. Deleuze*

Theoretical Chemistry, Department SBG, Hasselt University, Agoralaan, Gebouw D, B-3590 Diepenbeek, Belgium

Received: May 31, 2007; In Final Form: July 31, 2007

The potential energy surface of norbornane in its dicationic singlet ground state has been investigated in detail using density functional theory along with the nonlocal hybrid and gradient-corrected Becke three-parameter Lee−Yang−Parr functional (B3LYP) and the cc-pVDZ basis set. For the sake of more quantitative insight into the chemical reactions induced by double ionization of norbornane, this study was supplemented by a calculation of basic thermodynamic state functions coupled to a focal point analysis of energy differences obtained using correlation treatments and basis sets of improving quality, enabling an extrapolation of these energy differences at the CCSD(T) level in the limit of an asymptotically complete (cc-pV∞Z) basis set. Our results demonstrate the likelihood of an ultrafast intramolecular rearrangement of the saturated hydrocarbon cage after a sudden removal of two electrons into a kinetically metastable five-membered cyclic $C_5H_8^+$—CH^+—CH_3 intermediate, prior to a Coulomb explosion into $C_5H_7^+$═CH_2 and CH_3^+ fragments, which might explain a tremendous rise of electron-impact (e, 2e) ionization cross sections at electron binding energies around the double-ionization threshold. The first step is straightforward and strongly exothermic ($\Delta H_{298} = -114.0$ kcal mol^{-1}). The second step is also exothermic ($\Delta H_{298} = -10.2$ kcal mol^{-1}) but requires an activation enthalpy ($\Delta H^{\dagger}_{298}$) of 39.7 kcal/mol. The various factors governing the structure of this intermediate, such as electrostatic interactions, inductive effects, cyclic strains, and methylenic hyperconjugation interactions, are discussed in detail.

I. Introduction

Gas-phase dications[1−7] have received considerably less attention, from both experimental and theoretical viewpoints, than has been accorded to their monocationic counterparts. This is a consequence of the somewhat greater difficulties inherent in studies of doubly charged versus singly charged species. Molecular dications are subject to sizable electrostatic strains due to intramolecular Coulomb repulsions, as well as significant electronic or multireference correlation effects due to the more limited energy gaps between occupied and unoccupied orbital levels. Clearly, their formation necessitates larger ionization energies than the formation of monocations. In the condensed phase (either in solution or in the solid state), dications are stabilized by interactions with counterions, solvent molecules,[8] or appropriate ligands[9] that can accommodate the positive charges. In the gas phase, these stabilizing factors are missing, and the majority of small molecular dications (e.g., CF_2^{2+} or CF_3^{2+} [10]) are thermodynamically prone to Coulomb fragmentation processes, in order to release excessively strong electrostatic repulsions. Very few diatomic dications are thermodynamically stable in the gas phase.[5] In contrast, large cage compounds such as fullerenes[11] are known to exhibit exceptional stability[12] against charge fragmentation processes, because of their special structure and size. Multiply charged C_{60} ions can therefore be rather easily produced and characterized.[13]

Most gas-phase molecular dications are *kinetically* metastable.[5,6] More specifically, these molecular dications exist in long-lived states that are separated from the energy asymptotes for the dissociation products by sufficiently sizable energy barriers on the potential energy surface. These barriers are a consequence of the fact that chemical bonding can be strong enough to overcome the electrostatic repulsions between charge centers.[5,6] Somewhat counterintuitively, two-electron ionization events in weakly bound clusters of aromatic molecules have, for instance, been found to lead to the formation of large kinetically metastable assemblies[14] tightened by additional covalent bonds. In view of the combination of high kinetic stability and exceptional thermodynamic instability, many molecular dications can be regarded as "energy-rich" or "volcanic" systems that could represent a possible source of propulsion energy.[15]

Studies of carbenium dications are especially motivated by the fact that these species are produced exclusively by the removal of electrons from bonding orbitals in the neutrals. In the absence of conjugation with π- or lone-pair-donating substituents, the observed systems owe their existence to delocalizing interactions anchored to π conjugation, hyperconjugation, and aromaticity. Examples of experimentally known dicarbenium dications include the dications of ethylene,[16] cyclobutadiene,[17] norbornadiene,[18] and pagodanes.[19] An exceptionally stable dication is the 1,3-dehydro-5,7-adamantanediyl dication[20] that exhibits three-dimensional aromaticity due to the overlap of four C_{2p} orbitals in a tetrahedral fashion.

Bimolecular reactions of dications with neutral molecules are, furthermore, often merely dominated by electron transfer. The few known bond-forming reactions of molecular dications[21,22] are, by and large, limited to processes with concomitant electron transfer.[23] Fragmentation reactions of some arene dications[24−26] suggest, however, that medium-sized organic dications can react with neutral compounds, such as acetylene, without the occurrence of electron transfer.[27]

* Corresponding author. E-mail: michael.deleuze@uhasselt.be.

10.1021/jp074207r CCC: $37.00
Published on Web 10/04/2007

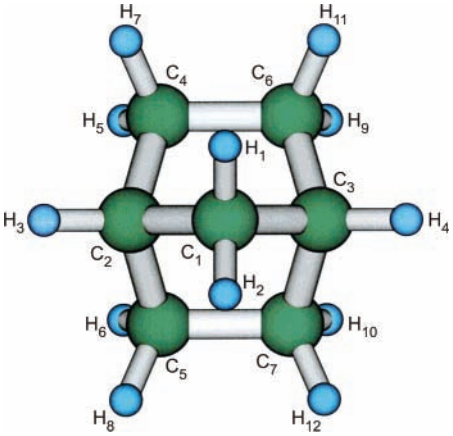

Figure 1. Norbornane in its neutral ground state. The nonredundant internal coordinates of this compound within the C_{2v} symmetry point group (B3LYP/cc-pVDZ geometry) are as follows: $R(C_1-C_2) = 1.54$ Å, $R(C_2-C_4) = 1.55$ Å, $R(C_4-C_6) = 1.56$ Å, $R(C_1-H_1) = 1.10$ Å, $R(C_2-H_3) = 1.10$ Å, $R(C_4-H_5) = 1.10$ Å, $R(C_4-H_7) = 1.10$ Å, $\theta(C_3-C_1-C_2) = 94.4°$, $\theta(C_1-C_2-C_4) = 101.5°$, $\theta(C_2-C_4-C_6) = 103.1°$, $\theta(H_1-C_1-C_2) = 113.3°$, $\theta(H_3-C_2-C_4) = 113.8°$, $\theta(H_5-C_4-C_6) = 112.8°$, $\theta(H_7-C_4-C_6) = 111.1°$, $\tau(H_5-C_4-C_6-C_3) = -120.9°$, $\tau(H_7-C_4-C_6-C_3) = 118.7°$.

The cage compound under investigation in this study is norbornane (C_7H_{12}). This molecule is a highly strained, bicyclic hydrocarbon exhibiting C_{2v} symmetry (Figure 1) that has proved useful in the therapy of cardiac infarctions as well as asthma, bronchitis, and thromboses.[28] Its molecular and electronic structures were already studied in the 1960s.[29,30] The outer-valence ionization spectrum of norbornane was recorded by Bishof et al.[31] and Getzlaff and Schönhense[32] by means of ultraviolet (He I) photoemission (UPS) spectroscopy. Bieri et al.[33] further investigated the inner valence ionization bands up to ~24 eV, using a He II photon beam.

Very recently, our group has been involved in an exhaustive study of the valence wave function of norbornane employing electron momentum spectroscopy (EMS).[34] The EMS spectrum and related momentum distributions were found to corroborate the available UPS measurements and 1p-GF calculations employing the benchmark third-order algebraic diagrammatic construction scheme [ADC(3)],[35−38] except for a particularly broad and intense band at 25 eV in the EMS spectrum that the 1p-GF/ADC(3) calculations failed to reproduce.[39] This striking discrepancy between theory and experiment has thereafter been referred to as the "band 12 issue".[40] It has led us to undertake further ADC(3) calculations with various basis sets[40] and to compare these to updated UPS measurements[40] by J. H. D. Eland (Oxford University) employing a 256 Å photon beam for binding energies of up to 40 eV. Except for a barely visible increase of the spectral background at ~26 eV that has been ascribed to the double-ionization threshold, the agreement between all theoretical ADC(3) results and the new experimental UPS data was almost perfect. Therefore, with regard to the characteristic time scales of ionization processes in EMS and UPS (10^{-17} versus 10^{-13} s, respectively), it has been suggested that ultrafast nuclear dynamical effects and Coulomb fragmentation processes induced by double ionization might be at the origin of the band at 25 eV in the EMS ionization spectrum. More specifically, shakeup states above the double-ionization threshold are expected to decay into dissociative shakeoff states within time scales on the order of 1 to a few tens of femtoseconds,[41,42] through relaxation of the excited electron into the inner-valence vacancy and auto-ionization of a second electron into the continuum (Figure 2).

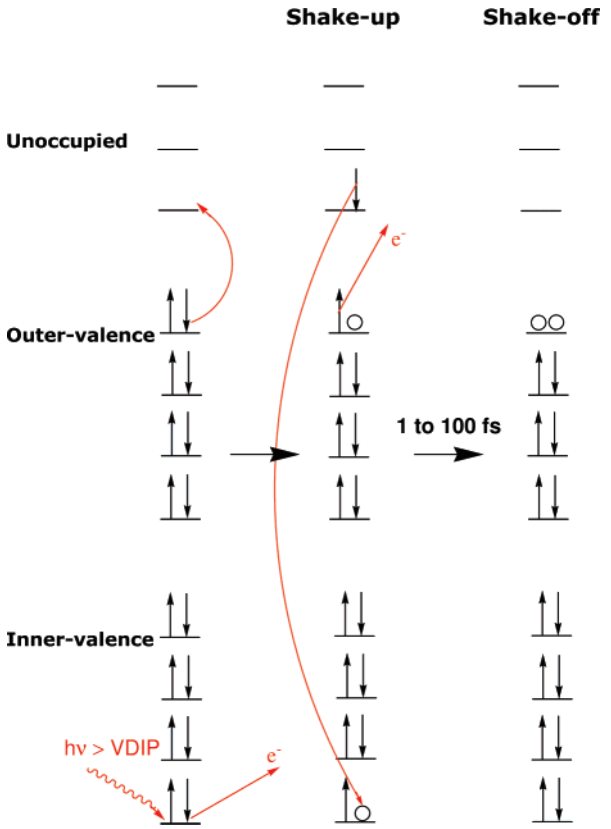

Figure 2. Intramolecular Coulomb decay of electronically excited shakeup states of norbornane^{2+} at the vertical double-ionization threshold of the neutral.

In straightforward analogy with the intermolecular Coulomb decay (ICD) mechanism, electric charges in dicationic species are expected to localize on separate fragments in order to minimize the extent of Coulomb repulsions. The ICD mechanism was proposed by Cederbaum et al.[41] for weakly bound clusters of molecules or noble gas atoms and has been confirmed experimentally for neon clusters.[43] Within a fully saturated hydrocarbon cage compound such as norbornane, all chemical bonds derive, according to a basic Lewis depiction, from the pairing of two electrons with opposite spins. In view of the importance of cyclic strains in the cage, the most important contribution of which arise from the $C_2-C_1-C_3$ bridge (Figure 1), it is therefore natural to expect, on intuitive chemical grounds, that a double-ionization event would induce the breaking of a single C−C bond. In other words, a purely electronic *intra*molecular Coulomb decay mechanism is expected to precede severe intramolecular rearrangements, once nuclear dynamics comes into play. The purpose of the present work is thus to test this hypothesis by studying in detail the potential energy surface (PES) of the dication of norbornane in its singlet ground state. In this work, we invoke the standard Born−Oppenheimer approximation, which enables us to compute the potential energy, $U(\{R_X\})$, of a fixed configuration of nuclei as the sum of the electronic energy obtained by solving the exact electronic Schrodinger equation ($H^{elec}\Psi^{elec} = E^{elec}\Psi^{elec}$) or, at least, an approximation to it, and of the nuclear repulsion energy ($\sum_{A,B} Z_A Z_B |R_A - R_B|^{-1}$).

II. Methodology Section

All geometry and frequency calculations presented in this work were performed using the Gaussian 98[44] quantum chemistry package. Density functional theory (DFT) was used in

conjunction with the nonlocal hybrid and gradient-corrected Becke three-parameter Lee−Yang−Parr functional (B3LYP),[45] along with Dunning's correlation-consistent polarized valence basis set of double-ζ quality (cc-pVDZ).[46] A default pruned integration grid with 75 radial shells per atom and 302 angular points per shell was used. The convergence of the results obtained with this grid was checked through comparisons with a few calculations of stationary points on the investigated potential energy surface, using an ultrafine pruned integration grid containing 99 radial shells per atom and 590 angular points.

Relaxation of the vertical doubly ionized state under the constraints of the C_{2v} point group was found to result into a second-order saddle point, referred to as S_2 (C_{2v}). This molecular structure was thereafter systematically distorted according to the normal vibrational modes characterized by imaginary frequencies, until first-order saddle points or energy minima could be reached. Transition states (TSs) for proton transfers were similarly identified by iteratively stretching the C−H bonds of interest via a scan of the potential energy surface, using the Molden graphical interface to construct suited *Z* matrices and letting geometries relax to first-order saddle points by means of the rational function optimization (RFO) method.[47] Enlarging the bridge of the C_{2v} structure of norbornane in its dicationic singlet ground state gave rise to the third-order saddle point S_3 (C_s), whose geometry was optimized using the synchronous transit-guided quasi-Newton method.[48,49] The expectation value of the S^2 operator was found to be zero. The stability of the spin-restricted wave function was also checked[50,51] for all identified stationary points through calculations of electronic excited states using the configuration interaction approach with singly excited determinants (CIS). In all cases, the wave functions were found to be electronically stable (i.e., all electronic excitation energies were of positive sign). In addition to this stability test, the single-reference nature of the wave function at the CCSD (coupled cluster with single and double excitations) level[52−55] of theory was also checked according to the T_1 diagnostic,[56] by means of the Molpro package.[57] All T_1 values were found to be less than 3.0% for each of the structures of interest, which typically reflects limited multireference effects. Finally, a few single-point calculations on test cases were performed at the complete active space self-consistent field (CASSCF)[58] level, using six active electrons in eight orbitals, in conjunction with the cc-pVDZ basis set, in order to evaluate the outcome of multireference effects. The weights of the main configurations were found to be over 90%, which again justifies a single-reference depiction for the wave function.

Harmonic vibrational frequencies and the related zero-point vibrational energies (ZPVEs) were analytically calculated throughout this work, to verify whether the identified stationary structures correspond to energy minima or to saddle points on the potential energy surfaces. Thermodynamic state functions (enthalpies, entropies, and Gibbs free energies) were obtained from Boltzmann's thermodynamic partition functions[59] calculated at the B3LYP/cc-pVDZ level at 298.15 K using the rigid rotor−harmonic oscillator (RRHO) approximation. Furthermore, natural bond orbital (NBO) analyses[60−67] were performed on all identified stationary points on the potential surface to investigate charge distributions.

Adiabatic ionization energies were computed as energy differences between the structurally optimized doubly ionized states and the neutral singlet ground state at the B3LYP/cc-pVDZ level using various many-body treatments of electron correlation on the corresponding B3LYP/cc-pVDZ geometries. The employed post-SCF treatments comprised MP2, MP3, and MP4SDQ (second, third, and partial fourth-order Møller-Plesset theory, respectively[68−72]) and CCSD and CCSD(T) [coupled cluster (CC) calculations employing the coupled cluster anzats for single (S) and double (D) electronic excitations, supplemented by a perturbative estimate[73] of triple (T) excitations].

Energy differences among the identified stationary points on the potential energy surface were accurately evaluated by a focal point analysis (FPA) similar to those carried out by Allinger et al.,[74] Salam et al.,[75] Kwasniewski et al.,[76] and Huang et al.,[77] to determine the conformational energy differences or barriers of *n*-butane, *n*-pentane, stilbene, and dimethoxymethane, respectively. The main feature of such an analysis is to determine, by pairing different levels of theory and basis sets, how the energy differences converge to the exact solution of the Schrödinger equation. To be more specific, one exploits for this purpose the faster convergence with respect to the basis set of the higher-order correlation corrections to the calculated energy differences in well-suited extrapolations of results of single-point calculations performed on the B3LYP/cc-pVDZ geometries using ab initio (HF and many-body) approaches and basis sets of improving quality. Reliable estimations of CCSD(T) energy differences in the limit of an exceedingly large basis set can then be made by adding almost-converged high-level correlation corrections, obtained at the MP3, CCSD, and CCSD(T) levels with rather limited basis sets, to lower-level HF and MP2 results that are calculated in conjunction with the largest basis sets, along with suitable extrapolation procedures. In the analysis, the employed basis sets were Dunning's correlation-consistent polarized valence double-, triple-, and quadruple-ζ basis sets, namely, cc-pVDZ, cc-pVTZ, and cc-pVQZ,[46] incorporating a total of 158, 378, and 745 atomic functions, respectively. These even-tempered basis sets enable an extrapolation of the HF/cc-pVXZ (X = D, T, Q) energies to the limit of an asymptotically complete (cc-pV∞Z) basis set with an exponential fit of the form

$$E(l) = E_\infty + A\mathrm{e}^{-Bl}$$

as was suggested by Feller.[78,79] In the above equation, the cardinal number l equals 2, 3, and 4, when X = D, T, and Q, respectively. The MP2/cc-pVXZ energies can be similarly extrapolated to the asymptotic limit of basis-set completeness using a three-point version [known as Schwartz 6(lmn)[80]] of Schwartz's extrapolation,[81] based on inverse powers of $(l + {}^1/_2)$, with $l = 2$, 3, and 4 when X = D, T, and Q, respectively.

$$E(l) = E_\infty + \frac{B}{\left(l+\frac{1}{2}\right)^4} + \frac{C}{\left(l+\frac{1}{2}\right)^6}$$

The key aspect of a focal point analysis (FPA) is to determine the basis set at which each of the successive corrections evaluated by the various ab initio methods has converged within a satisfactory threshold. With such a procedure, it is then possible to extrapolate benchmark CCSD(T) results to the asymptotically complete cc-pV∞Z basis set, which enables, for instance, a determination of conformational energy differences within an accuracy of ∼0.05 kcal/mol[75−77] or ionization energies within an accuracy of ∼0.04 eV.[82]

Many thorough studies have shown that DFT, in conjunction with standard hybrid and gradient-corrected (GGA) functionals such as B3LYP, is suited for semiquantitative calculations of reaction and activation energies (enthalpies), i.e., within relative accuracies of ∼10% for energy differences.[83−86] The B3LYP functional is nonetheless known to substantially underestimate

TABLE 1: Calculations of the Vertical and Adiabatic Double-Ionization Potentials (VDIP and ADIP, Respectively) of Norbornane Considering Various Possible Energy Minima on the Potential Energy Surface of Norbornane^{2+} in Its Singlet Ground State[a]

		ADIP				
	VDIP	S_2 (C_{2v})[b]	C5-Min$_1$	C5-Min$_2$	C5-Min$_3$	C6-Min$_4$ (C_s)
HF	27.178	24.021	19.548	19.842	20.240	19.125
MP2	25.941	23.516	21.726	21.998	22.225	21.314
MP3	26.873	24.214	21.493	21.768	22.086	21.069
MP4[c]	26.995	24.312	21.470	21.740	22.070	21.054
CCSD	26.965	24.301	21.442	21.714	22.047	21.034
CCSD(T)	26.503	23.963	21.487	21.748	22.066	21.084
B3LYP	26.218	23.813	21.163	21.338	21.891	20.648

[a] Results in eV, obtained using the cc-pVDZ basis set and B3LYP/cc-pVDZ geometries. [b] Given for the sake of comparison, as a rough estimate of the adiabatic double-ionization potential *prior* to bond breaking.[40] [c] Fourth-order Møller-Plesset perturbation theory, using the space of single, double and quadruple substitutions.

energy barriers for unimolecular rearrangement reactions. As an alternative, use was also made of the modified Perdew−Wang one-parameter model for kinetics (MPW1K)[83,87] for exploring the potential energy surface of norbornane^{2+} in its singlet ground state. This hybrid functional is characterized by a higher fraction of Hartree−Fock exchange than B3LYP, which normally helps describing the electron delocalization induced by bond stretching in a more reliable way. MPW1K was thus shown to provide improved energy barriers,[84,88,89] but at the expense of the quality of the geometries of saddle points. For the sake of completeness, we were thus willing to calibrate the two functionals from a comparison of the results of B3LYP/cc-pVDZ and MPW1K/cc-pVDZ calculations with benchmark CCSD(T) and FPA data, considering both single-point calculations on B3LYP/cc-pVDZ geometries and full optimization runs at the MPW1K/cc-pVDZ level, in order to assess the influence of the geometry of the identified stationary points on the quality of the computed energy differences.

III. Results and Discussion

1. Potential Energy Surface. *A. Relaxation of Doubly Ionized Norbornane to Five-Membered Monocyclic Intermediates (C5-Min$_x$, x = 1−3).* Adiabatic ionization energies corresponding to the most important stationary points identified on the potential energy surface of norbornane^{2+} in its singlet ground state are reported in Table 1 and compared to the vertical double-ionization potential. At the B3LYP/cc-pVDZ level, under the constraint of C_{2v} symmetry, geometric relaxation of this singlet dicationic species was found to yield a second-order saddle point, referred to as S_2 (C_{2v}). This stationary point defines the central entry on our conformational energy map displayed in Figure 3, obtained by sketching the evolution of the potential energy $U(\{R_X\})$ of the doubly ionized molecule as a function of structural distortions measured by the two vibrational modes $\boldsymbol{q_1}$ and $\boldsymbol{q_2}$ that are characterized by imaginary frequencies (426i and 365i cm^{-1}). Compared to the vertical doubly ionized state, geometry relaxation was found at the same level (Table 2) to release an energy of 2.41 eV or 55.57 kcal/mol. From this point, vibrations along the $\boldsymbol{q_1}$ and $\boldsymbol{q_2}$ modes and subsequent geometry optimization under the constraints of C_s symmetry point groups enable energy relaxation (i.e., a lowering of the potential energy $U(\{R_X\})$ into four directions, which divide the conformational energy map into four symmetry-equivalent quadrants (Figure 3). Figure 4 is equivalent to one of these quadrants. Upon

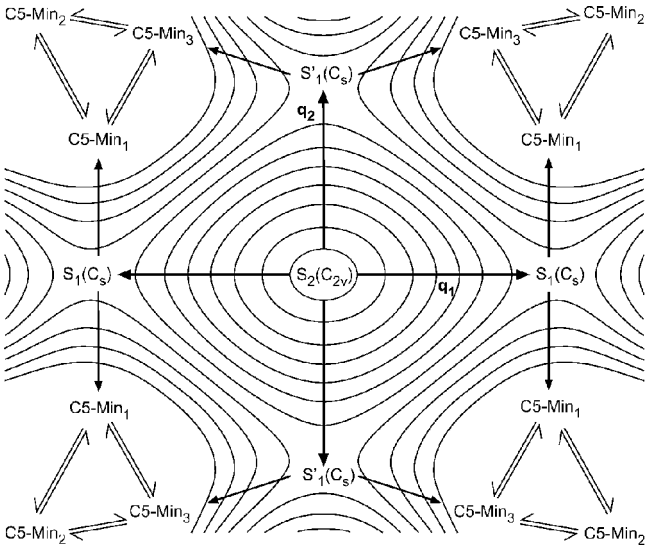

Figure 3. Sketch of the potential energy surface of norbornane^{2+} in its singlet ground state.

analysis of the NBO charge distributions (Table 3) in the S_2 (C_{2v}) species (Figure 4a), it is clear that, in this highly symmetric but unstable structure, the charges are merely delocalized over the outermost hydrogens (H_7, H_8, H_{11}, H_{12}) and over the bridgehead carbons C_2 and C_3. Upon comparison of the total electric charge ascribed to the carbon backbones of the S_2 (C_{2v}) structure to that for the neutral, singlet C_{2v} structure of norbornane (see Table 4), it also appears that +0.48*e* or only about one-fourth of the double positive charge is effectively localized on the carbon backbone of the system.

A potential energy lowering of 17.43 kcal/mol (Table 2) is observed when the S_2 (C_{2v}) structure is distorted and relaxed upon the constraint of the C_s symmetry plane that contains the C and H atoms in the bridge methylenic group (H_1, C_1, and H_2). The obtained transition state [S′$_1$ (C_s) in Figure 4b] is a strongly stretched structure consisting of an ethylene molecule (C_2H_4) bound via charge transfer to a five-membered cyclic dicarbenium dication ($C_5H_8^{2+}$). Indeed, the covalent bond order of the C_4−C_6 bond, as defined by Wiberg,[90] was found to be equal to 1.718. The ethylene fragment borrows a substantial fraction of the double positive charge (+0.36*e*), whereas an absolute NBO charge of +1.64*e* remains localized on the five-membered ring. Comparison of the NBO charges in the S′$_1$ (C_s) species to those of norbornane in its neutral ground state indicates that, in this S′$_1$ (C_s) species, the double positive charge ascribed to the removal of two electrons predominantly localizes on atoms C_2 and C_3 (Table 4).

Both this observation and the almost-planar configuration of substituents attached to atoms C_2 and C_3 corroborate the idea of an sp^2 hybridization state and the presence of an empty C_{2p} orbital on these atoms. More specifically, the C_1−C_3−H_4−C_7 dihedral angle amounts to 166.7°. The interatomic distances C_2−C_4 and C_3−C_6 were found to be equal to 2.65 Å, a value to compare to the C_2−C_5 or C_3−C_7 bond lengths of 1.46 Å. Clearly, symmetry lowering and bond breaking at this stage can already lead to a localization of charges, which precedes the expected Coulomb fragmentation.

In contrast to this first distortion, distorting and relaxing the S_2 (C_{2v}) structure under the constraint of the symmetry plane containing the atoms C_1, C_2, and C_3 enables a (potential) energy lowering by 4.62 kcal/mol only at the B3LYP/cc-pVDZ level (Table 2). A comparison of the charge distribution (Table 3) in the resulting species S_1 (C_s) (Figure 4c) to that of the neutral

TABLE 2: Energies (kcal mol^{-1}) of the Identified Stationary Points on the Potential Energy Surface of Norbornane^{2+} in Its Singlet Ground State Obtained with a Variety of Methods along with the cc-pVDZ Basis Set, Relative to the $C_5H_8^+$—CH^+—CH_3 Energy Minimum (C5-Min$_1$)

structure	B3LYP[a]	MPW1K[a]	MPW1K[b]	CCSD(T)[a]	CCSD(T)[b]	FPA[a,c]
S_2 (C_{2v})	61.12	63.94	63.51	57.09	57.77	55.71
S'_1 (C_s)	43.69	51.61	51.37	45.04	44.43	43.37
S_1 (C_s)	56.50	49.10	41.94	47.80	41.27	45.86
C5-Min$_1$	0.00	0.00	0.00	0.00	0.00	0.00
C5-Min$_2$	4.05	4.60	4.68	6.01	6.06	5.33
TS_1^{PT}	6.02	5.09	5.33	5.54	6.10	4.99
C5-Min$_3$	16.79	15.44	–	13.34	–	11.17
TS_2^{PT}	18.39	14.20	–	13.29	–	12.56
TS_3^{PT}	19.33	19.86	–	16.46	–	16.92
TS^{Dis}	41.45	49.73	49.78	40.56	40.80	41.71
S_3 (C_s)	92.06	100.61	–	93.35	–	93.58
C6-Min$_4$ (C_s)	−11.87	−11.87	−11.77	−9.29	−9.23	−10.16
$C_5H_7^+$═CH_2 + CH_3^+	−2.82	0.91	1.06	−9.08	−8.94	−7.77

[a] Based on B3LYP/cc-pVDZ geometries. [b] Based on MPW1K/cc-pVDZ geometries. [c] Extrapolated CCSD(T)/cc-pV∞Z data; see Table 5 for details.

C_{2v} structure of norbornane indicates (Table 4) a rather pronounced localization of charges produced by double ionization on C_3, H_{11}, and H_{12} and, to a lesser extent, over H_9, H_{10}, C_6, and C_7. The overall pattern is therefore a localization of one of the two positive charges within the most strongly stretched and angularly distorted part of the molecule (on the right-hand side of Figure 4c). More specifically, the distortions in this species amount to a stretching of the C_3—C_6 (or, through symmetry, C_3—C_7) bonds from 1.63 Å in the S_2 (C_{2v}) structure to 1.66 Å for the in S_1 (C_s) one, along with a decrease of the C_7—C_3—C_6 angle from 93.6° to 68.1°. In contrast, and in line with the decrease of the charge density in the region defined by the left-hand side of Figure 4c, the C_2—C_4 and C_2—C_5 bond lengths decrease from 1.67 to 1.55 Å, whereas the corresponding C_5—C_2—C_4 bond angle increases from 93.6° to 102.0°. For the sake of comparison, it is worth mentioning that, at the same level, norbornane in its neutral and singlet ground state is characterized by C_4—C_2—C_5 and C_3—C_6—C_7 bond angles that are equal to 108.5°, with values of 1.57 and 1.55 Å for the C_4—C_6 (C_5—C_7) and C_2—C_4 (C_2—C_5) bond lengths, respectively.

Upon distortion of the S_1 (C_s) saddle point according to the vibrational mode associated with the imaginary frequency (296i cm^{-1}), the C_3—C_6 bond was found to break and to release, at the B3LYP/cc-pVDZ level, an energy of 56.50 kcal/mol (Table 2) after relaxation into the C5-Min$_1$ species (Figure 4d). The latter structure defines the global energy minimum in the series of all identified structures with a five-membered (C5) ring, hence its working name. After cleavage of the C_3—C_7 bond, two proton transfers were observed during the relaxation process, the first from C_6 to C_7 and the second from C_2 to C_4, according to the atom labeling used in Figure 4d. The doubly positive charged product is a $C_5H_8^+$ ring bearing a 1-dehydroethyl cation substituent (CH^+—CH_3) in the γ position relative to the charge center in the ring. In this structure, the largest positive partial charges are located on the C_2 and C_6 carbons. This structure and the above-mentioned energy release of 56.50 kcal/mol are the result of a balance between a minimization of the electrostatic Coulomb repulsion and a maximization of stabilizing effects such as hyperconjugation interactions between C—H bonds and empty C_{2p} orbitals, as well as inductive effects that tend to favor localization of charges on carbocations bearing the maximum number of hydrogen substituents. The latter argument is consistent with Markovnikov's rule,[91] which states that a highly substituted carbocation is more stable than a less substituted one. Hyperconjugation interactions are directly reflected by the values found for the C_3—C_6—H_9—C_7 and H_4—C_3—C_6—H_9 dihedral angles (176.2° and −84.4°, respectively), from which one can infer in particular that the C_3—H_4 bond lies parallel to the nearby empty C_{2p} orbital. In addition, departures from planarity for the $C_5H_8^+$ ring remain limited, which favors through-space methylenic hyperconjugation interactions[92] between approximately parallel C—H bonds: the C_1—C_2—C_4—C_5, C_2—C_4—C_5—C_3, C_1—C_3—C_5—C_4, C_2—C_1—C_3—C_5, and C_3—C_1—C_2—C_4 angles, for instance, are equal to −8.2°, 19.5°, −23.3°, 19.0°, and −6.9°, respectively.

Enforcing a proton transfer (PT) between the C_3 and C_6 atoms in the C5-Min$_1$ species results in a second minimum referred to as C5-Min$_2$ (Figure 4e), in which an ethyl group is attached to one of the carbocationic centers of the cyclic $C_5H_7^{2+}$ structure. This structures lies 4.05 kcal/mol above the C5-Min$_1$ species (Table 2). In the C5-Min$_2$ structure, holes are located rather close to each other on C_2 and C_3 in an almost-planar $C_5H_7^{2+}$ cyclic ring [in this ring, the largest dihedral angle (C_1—C_3—C_5—C_4) amounts to 5.8° only]. This species is, according to Markovnikov's rule,[91] more effectively stabilized than C5-Min$_1$ by inductive effects around the tertiary carbenium atom (C_3), but at the expense of stronger electrostatic repulsions between the charge centers. Here also, hyperconjugation between the C_6—H_8 bond and the empty C_{2p} orbital on C_3 plays an important role, as the C_1—C_3—C_6—H_8 dihedral angle amounts to 78.7°. Note in particular that the Wiberg bond index of C_3—C_6 and the corresponding bond length amount to 1.26 and 1.44 Å, respectively. The transition state for this proton transfer is TS_1^{PT} (Figure 5) defining an energy barrier of only 1.97 kcal/mol (Table 2) relative to the C5-Min$_2$ species. In line with this result and the endothermicity of the transformation from C5-Min$_1$ to C5-Min$_2$, the structure of TS_1^{PT} was found to resemble that of C5-Min$_2$, in agreement with Hammond's principle.[91] For TS_1^{PT}, the transferred proton (H_8) was found to be 1.47 and 1.26 Å from the C_3 and C_6 atoms, respectively. The C_3—H_8 and C_6—H_8 Wiberg bond indices correspondingly amount to 0.309 and 0.469, respectively.

The C5-Min$_3$ minimum (Figure 4f) was found upon distortion of the S'_1 (C_s) structure according to the mode associated with the imaginary frequency (232i cm^{-1}). This geometry relaxation results in an energy lowering of 26.90 kcal/mol (Table 2). The S'_1 (C_s) structure can be described as a $C_5H_8^+$ ring bearing, this time, a 2-dehydroethyl cation substituent (CH_2—CH_2^+) in the γ position relative to the charge center in the ring. In this structure, electrostatic repulsion between the charge centers is

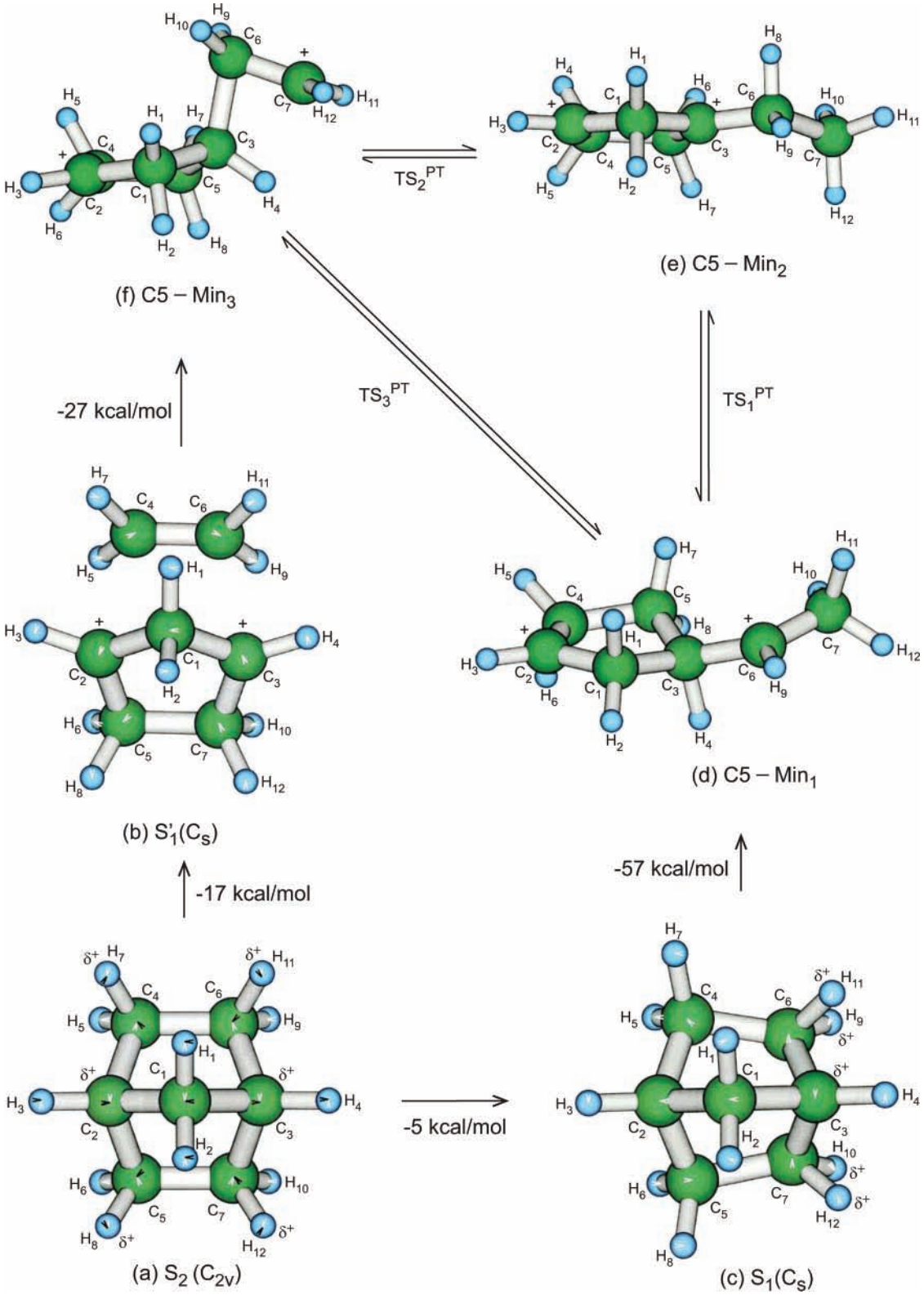

Figure 4. B3LYP/cc-PVDZ study of a nonredundant part of the potential energy surface of norbornane^{2+} in its singlet ground state. Darts provide the atomic displacements associated with the vibrational eigenmodes characterized by imaginary frequencies. The δ^+ and + symbols indicate moderate and strong localization of the charges created by double ionization, in line with the values reported in bold in Tables 3 and 4. See Figure 5 for the transition states describing proton transfers. The reported energy variations are B3LYP/cc-pVDZ results. See text for more accurate estimates.

clearly minimized, as the distance between the C_2 and C_7 atoms is equal to 4.27 Å, compared to the 3.39 Å separating the C_2 and C_6 atoms. On the other hand, the disadvantage here lies at the level of much less favorable inductive effects around a primary carbenium atom (C_7), in line with Markovnikov's rule. Despite an interdistance of 1.94 Å between the H_4 and C_7 atoms, hyperconjugation between the C_3—H_4 bond and the nearby empty C_{2p} atomic orbital on C_7 is inferred from the H_4—C_3—C_6—C_7 dihedral angle (−0.2°), from the unusually low value of 81.0 ° found for the C_3—C_6—C_7 bond angle, and from a

TABLE 3: Natural Population Analysis of the Electronic Density for All Identified Stationary Points on the Potential Surface of Norbornane^{2+} in Its Singlet Ground State, Compared to That of the Neutral Species[a]

	neutral[b]	S_2 (C_{2v})	S'_1 (C_s)	S_1 (C_s)	C5-Min_1	C5-Min_2	TS_1^{PT}	C5-Min_3	TS_2^{PT}	TS_3^{PT}	TS^{Dis}	S_3 (C_s)	C6-Min_4 (C_s)	CH_3^+	$C_5H_7^+$=CH_2
C_1	−0.445	−0.491	−0.591	−0.493	−0.542	−0.632	−0.593	−0.546	−0.550	−0.566	−0.571	**−0.148**	−0.721	0.295	−0.537
C_2	−0.245	**−0.090**	**0.239**	−0.217	**0.329**	**0.350**	**0.341**	**0.326**	**0.333**	**0.320**	**0.316**	−0.169	**0.450**	−	**0.273**
C_3	−0.245	**−0.090**	**0.239**	**0.000**	−0.357	**0.435**	**0.146**	−0.253	**−0.145**	−0.203	0.030	−0.188	**0.319**	−	−0.078
C_4	−0.444	−0.392	−0.342	−0.470	−0.548	−0.570	−0.562	−0.555	−0.550	−0.559	−0.539	−0.387	−0.543	−	−0.524
C_5	−0.444	−0.392	−0.541	−0.470	−0.442	−0.540	−0.496	−0.430	−0.434	−0.440	−0.472	−0.387	−0.568	−	−0.454
C_6	−0.444	−0.392	−0.342	−0.332	**0.310**	−0.525	**−0.256**	−0.424	−0.413	−0.578	−0.359	−0.433	−0.568	−	−0.320
C_7	−0.444	−0.392	−0.541	−0.332	−0.746	−0.652	−0.672	**0.037**	**−0.204**	**0.258**	**0.124**	−0.433	−0.543	−	−
H_1	0.224	0.309	0.344	0.333	0.362	0.391	0.398	0.338	0.347	0.323	0.338	0.288	0.308	0.235	0.368
H_2	0.224	0.309	0.379	0.333	0.344	**0.411**	0.367	0.379	0.372	0.384	0.372	0.288	0.308	0.235	0.319
H_3	0.237	0.328	0.313	0.327	0.301	0.308	0.306	0.302	0.305	0.296	0.289	0.345	0.360	0.235	0.273
H_4	0.237	0.328	0.313	0.352	0.376	0.399	0.377	0.341	**0.388**	0.294	0.377	0.359	0.296		0.312
H_5	0.222	0.327	0.262	0.313	0.358	0.388	0.395	0.381	0.391	0.375	0.342	0.355	0.362		0.348
H_6	0.222	0.327	0.356	0.313	0.386	0.355	0.331	0.364	0.366	0.363	0.293	0.355	0.362		0.265
H_7	0.225	**0.415**	0.258	0.325	0.278	0.364	0.323	0.289	0.296	0.288	0.290	**0.370**	0.334		0.277
H_8	0.225	**0.415**	0.389	0.325	0.294	0.388	**0.418**	0.292	0.290	0.299	0.241	**0.370**	0.334		0.243
H_9	0.222	0.327	0.262	**0.387**	0.276	0.323	0.311	0.297	0.298	0.336	0.242	**0.392**	0.374		0.235
H_{10}	0.222	0.327	0.356	**0.387**	0.286	0.248	0.257	0.291	0.292	0.304	0.229	**0.392**	0.374		−
H_{11}	0.225	**0.415**	0.258	**0.461**	0.378	0.292	0.309	0.286	0.311	0.267	0.230	0.315	0.380		−
H_{12}	0.225	**0.415**	0.389	**0.461**	0.357	0.268	0.299	0.283	0.307	0.240	0.229	0.315	0.380		−

[a] B3LYP/cc-pVDZ results. Bold values reflect moderate and strong localization of the charges created by double ionization, as indicated by δ^+ and + symbols, respectively, in Figures 4−6, 8, and 9. Also see Figures 4−6, 8, and 9 for atom labeling. [b] B3LYP/cc-pVDZ natural population analysis of norbornane in its neutral ground-state singlet C_{2v} structure. See Figure 1 for atom labeling.

TABLE 4: Charge Differences Obtained from a Natural Population Analysis of the Electronic Density of a Few Stationary Points on the Potential Energy Surface of Doubly Ionized Norbornane in Its Singlet Ground State Compared to That of the Neutral in Its Singlet Ground State[a]

	S_2 (C_{2v})	S'_1 (C_s)	S_1 (C_s)	S_3 (C_s)	C6-Min_4 (C_s)
C_1	−0.046	−0.146	−0.048	**0.297**	−0.276
C_2	**0.155**	**0.484**	0.028	0.076	**0.695**
C_3	**0.155**	**0.484**	**0.245**	0.057	**0.564**
C_4	0.052	0.102	−0.026	0.057	−0.099
C_5	0.052	−0.097	−0.026	0.057	−0.124
C_6	0.052	0.102	0.112	0.011	−0.124
C_7	0.052	−0.097	0.112	0.011	−0.099
H_1	0.085	0.120	0.109	0.064	0.084
H_2	0.085	0.155	0.109	0.064	0.084
H_3	0.091	0.076	0.090	0.108	0.123
H_4	0.091	0.076	0.115	0.122	0.059
H_5	0.105	0.040	0.091	0.133	0.140
H_6	0.105	0.134	0.091	0.133	0.140
H_7	**0.190**	0.033	0.100	0.145	0.109
H_8	**0.190**	0.164	0.100	0.145	0.109
H_9	0.105	0.040	0.165	**0.170**	0.152
H_{10}	0.105	0.134	0.165	**0.170**	0.152
H_{11}	**0.190**	0.033	**0.236**	0.090	0.155
H_{12}	**0.190**	0.164	**0.236**	0.090	0.155

[a] B3LYP/cc-pVDZ results.

Wiberg bond index of 0.794 for the C_3—H_4 bond, indicating that this bond is partly deprived of its electron density. Thus, hyperconjugation here obviously develops at the expense of much more pronounced angular strains. All in all, this energy minimum is thus found to lie at ∼16.8 kcal/mol above the C5-Min_1 global energy minimum. From Figure 3, it is then clear that the S_2 (C_{2v}) structure defining the central second-order saddle point on the potential energy map will predominantly relax into the C_5-min_1 structure, when following the steepest energy gradients without any control on symmetry.

An additional pathway connecting the C5-Min_2 and C5-Min_3 minima could be identified via the transition state TS_2^{PT}, which coincides with a proton transfer from C_3 to C_7 (Figure 5b). This transition state lies 14.34 and 1.60 kcal/mol above C5-Min_2 and C5-Min_3, respectively. It can be noticed from Figure 5b that, as in the C5-Min_3 species to which it is closely related by virtue of Hammond's principle, the ethyl tail of TS_2^{PT} is subject to considerable angular strains. In this structure, the C_3—H_4 and C_7—H_4 bond lengths and the C_3—C_6—C_7 bond and C_1—C_3—C_6—C_7 torsion angles amount to 1.23 Å, 1.42 Å, 74.4°, and 113.3°, respectively. In this structure, the H_4—C_3—C_6—C_7 torsion angle remains equal to 0°. The Wiberg bond indices for the C_3—H_4, C_7—H_4, and C_3—C_7 atomic pairs are correspondingly equal to 0.524, 0.286, and 0.477.

The C5-Min_3 species transforms into the global energy minimum form (C5-Min_1) among five-membered cyclic species via the TS_3^{PT} saddle-point structure of Figure 5c. The latter species lies 2.54 kcal mol^{-1} above C5-Min_3 and essentially differs from it by an opening of the C_3—C_6—C_7 bond angle from 81.0° (C5-Min_3) to 111.9° (TS_3^{PT}). This opening implies a breaking of bonding interactions due to hyperconjugation between the C_3—H_4 bond and the empty C_{2p} atomic orbital on C_7, along with rotation of the end methylene group (C_7, H_{11}, H_{12}) about the C_3—C_6 bond in order to minimize electrostatic and steric repulsions: after rotation, for TS_3^{PT}, the C_2—C_7 interatomic distance and C_1—C_3—C_6—C_7 torsion angle are equal to 4.41 Å and 111.9°. In this transition state, the migrating hydrogen atom (H_9) remains closely bound to C_6; the C_6—H_9 bond length and the corresponding Wiberg index amount to 1.11 Å and 0.806, respectively. In contrast, the bond index of C_6—C_7 was found to be 1.274.

B. Charge Fragmentation of Five-Membered Monocyclic Intermediates. In the next step, dissociation can occur at the B3LYP/cc-pVDZ level through a heterolytic breaking of the C_6—C_7 bond in the $C_5H_7^{2+}$—CH_2—CH_3 (C5-Min_2) structure (Figure 6a), giving rise to a methyl cation (CH_3^+) and to a $C_5H_7^+$=CH_2 cation with the charge center in the γ position relative to the carbon atom bearing the methylene substituent (Figure 6b). This depiction is in line with the charge distributions reported in Table 3; with the relative orientation of substituents around the C_2, C_3, and C_6 atoms; and with a Wiberg covalent bond index of 1.911 for the C_3—C_6 bond in $C_5H_7^+$=CH_2. The transition state for this bond breaking was first roughly identified by studying the potential energy curve associated with a progressive stretching of the C_6—C_7 bond in the $C_5H_8^+$—CH^+—CH_3 (C5-Min_1) species, using a step size of 0.05 Å for the scan.

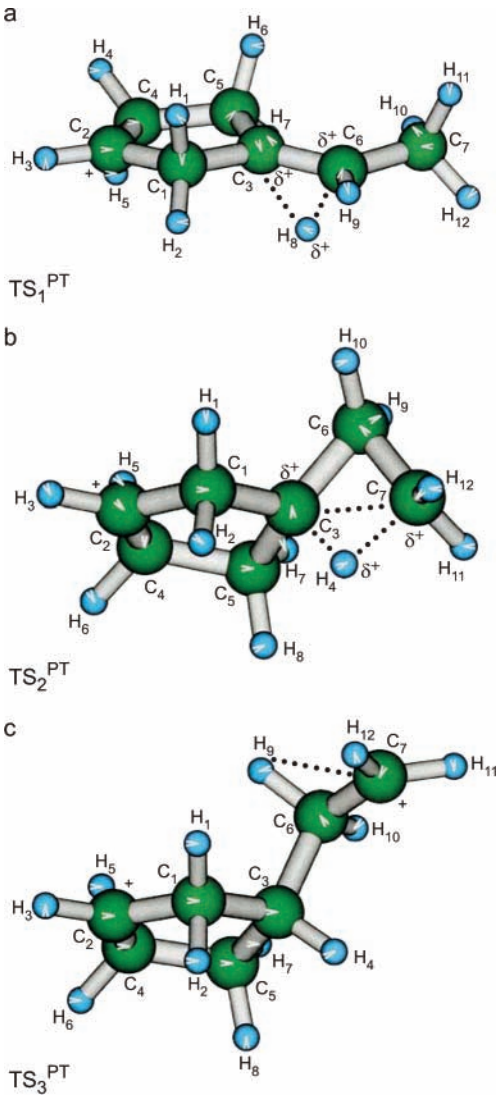

Figure 5. Transition states describing proton transfers (B3LYP/cc-pVDZ structures). Darts provide the atomic displacements associated with the vibrational eigenmodes characterized by imaginary frequencies. The δ^+ and + symbols indicate moderate and strong localization of the charges created by double ionization, in line with the values reported in bold in Tables 3 and 4.

During the elongation, we observed a hydrogen transfer from C_3 to C_6 at C_6—C_7 bond lengths ranging from 1.68 to 1.73 Å. The elongation process was continued until an energy maximum was clearly reached. Optimization of the structure characterizing this maximum under the constraint of one negative curvature led to the TS^{Dis} structure displayed in Figure 6a. In this structure, C_3—C_6 is already very close to a double bond (with a Wiberg bond index of 1.778). A residual bond between C_6 and C_7 remains partially preserved with a Wiberg bond index of 0.169, and the bond length between these two carbon atoms amounts to 3.68 Å.

At the B3LYP/cc-pVDZ level, the activation enthalpy for proton transfer from the $C_5H_8^+$—CH^+—CH_3 (C5-Min_1) species to the $C_5H_7^{2+}$—CH_2—CH_3 (C5-Min_2) species was found to be 4.58 kcal/mol (zero-point vibrational energies and thermal corrections included), whereas the activation enthalpy for the subsequent fragmentation of $C_5H_7^{2+}$—CH_2—CH_3 (C5-Min_2) to $C_5H_7^+$=CH_2 + CH_3^+ correspondingly amounted to 36.14 kcal mol^{-1} (see Figure 7). Provided that thermal equilibrium with the environment is reached, the $C_5H_8^+$—CH^+—CH_3 and $C_5H_7^{2+}$—CH_2—CH_3 species will both be extremely long-lived with respect

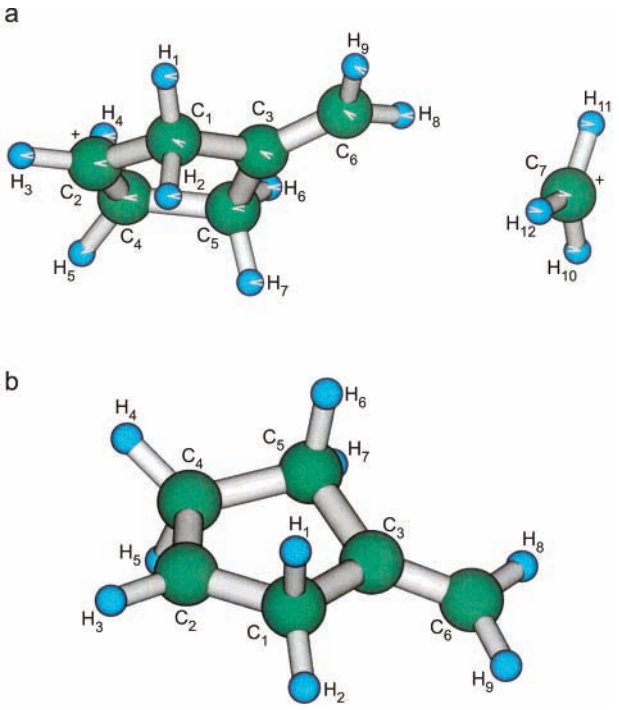

Figure 6. (a) Transition state and (b) product of the radical (homolytic) dissociation of $C_5H_8^+$—CH^+—CH_3 intermediate (the C5-Min_1 reference) into $C_5H_7^+$=CH_2 and CH_3^+ (B3LYP/cc-pVDZ results). Darts provide the atomic displacements associated with the vibrational eigenmodes characterized by imaginary frequencies. The + symbols indicate strong localization of the charges created by double ionization, in line with the values reported in bold in Tables 3 and 4.

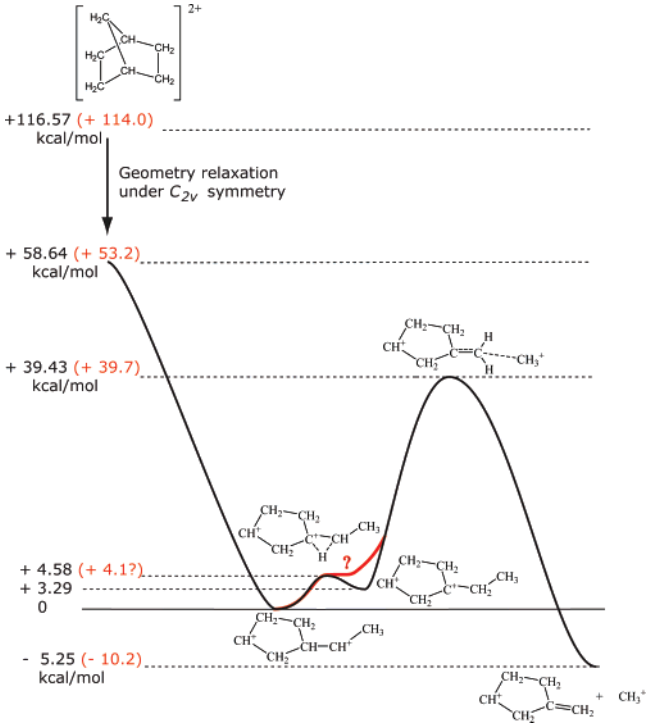

Figure 7. B3LYP/cc-pVDZ (black) and extrapolated CCSD(T)/cc-pV∞Z (red) potential energy pathways associated with relaxation of the vertical doubly ionized singlet ground state of norbornane^{2+} into the kinetically metastable $C_5H_8^+$—CH^+—CH_3 (C5-Min_1) intermediate and fragmentation of the latter into $C_5H_7^+$=CH_2 and CH_3^+ through stretching of the C_6—C_7 chemical bond. The reported values are enthalpy differences relative to the C5-Min_1 intermediate.

to charge fragmentation, whereas they will be subject to rapid interconversions via proton transfers. Typically, according to

transition state theory,[93] using the RRHO partition functions, the related unimolecular reaction rate constants associated at 298 K with the above barriers were estimated to be 6.7×10^9 and 5.2×10^{-11} s^{-1}, respectively. The corresponding half-lives amounted to ~0.10 ns and ~426 years. Note that, on the B3LYP/cc-pVDZ energy surface (Figure 7), the $C_5H_7^{2+}$—CH_2—CH_3 (C5-Min_2) species corresponds to a very shallow energy minimum. In line with the proton transfer from C_3 to C_6 induced upon stretching of the C_6—C_7 bond in the C5-Min_1 species (see above), it is thus worth mentioning that refinement (see further) of the potential energy surface from single-point calculations on B3LYP/cc-pVDZ geometries at the benchmark CCSD(T)/cc-pVDZ level or at an extrapolated CCSD(T)/cc-pV∞Z level (see Table 2) seems to indicate that, on the corresponding potential energy surfaces, the $C_5H_7^{2+}$—CH_2—CH_3 (C5-Min_2) species and related TS_1^{PT} transition would become almost isoenergetic, in which case these structures would essentially coincide (Figure 7) with a thermodynamically insignificant shoulder on a huge energy barrier, on the order of 41 kcal/mol, associated with a straightforward fragmentation of $C_5H_8^+$—CH^+—CH_3 into $C_5H_7^+$═CH_2 and CH_3^+. With such a scenario, considering our best estimate for the activation enthalpy (ZPVEs and thermal corrections included) and a TST value of $\sim 2.4 \times 10^{-13}$ s^{-1} for the associated rate constant, the $C_5H_8^+$—CH^+—CH_3 species would then be characterized by a half-life of $\sim 9 \times 10^4$ years at room temperature. More detailed and costly calculations involving full geometry optimizations at the CCSD(T)/cc-pVDZ level or beyond would be needed to investigate the potential energy surface of norbornane^{2+} within subchemical accuracy ($\Delta E = 0.1$ kcal/mol) and discriminate which of the two scenarios displayed in Figure 7 is correct.

Regardless of the final answer to this issue, it is clear that the initial state in the process is very far from equilibrium, considering the potential energy of ~114 kcal/mol [CCSD(T)/cc-pV∞Z estimate] that can be converted into kinetic forms (rotational, vibrational, and translational) of energy through a relaxation of the vertically doubly ionized singlet form of norbornane into the kinetically metastable $C_5H_8^+$—CH^+—CH_3 (C5-Min_1) intermediate and subsequent dissociation of the cage into smaller fragments. After double ionization of norbornane, enough energy will thus certainly be available for overcoming all the energy barriers (see Tables 1 and 2) on the reaction pathways leading to charge fragmentation of this intermediate into $C_5H_7^+$═CH_2 and CH_3^+. Because the reaction is sufficiently exothermic ($\Delta E = -7.8$ kcal/mol and $\Delta H_0 = -11.3$ kcal/mol, according to our best estimates; see further), this fragmentation will be spontaneous and irreversible under high-vacuum conditions. Therefore, at least one efficient and straightforward path for the fragmentation of norbornane^{2+} into two distinct monocationic species has been found, which provides support for the scenario invoked to tentatively explain the origin of band 12 in the EMS ionization spectrum of norbornane (see the Introduction).

Another likely charge dissipation pathway implies dissociation of the C5-Min_1 intermediate into $C_5H_8^+$ and $C_2H_4^+$ doublet radical cations; this reaction is indeed only slightly endothermic ($\Delta E = 3.87$ kcal/mol) at the B3LYP/cc-pVDZ level. Other reaction paths have been similarly tested, but at first glance, they seem less interesting from a thermodynamic viewpoint. The C5-Min_2 singlet dicationic species can dissociate into singlet $C_5H_7^+$ and $C_2H_5^+$ radical cations under a more substantial energy input of 23.88 kcal/mol. Also, an energy of 46.81 kcal/mol is required for dissociation of the C5-Min_3 dication into $C_5H_8^{2+}$ and C_2H_4 in their singlet ground states.

For comparison purposes, we would like to mention that the dissociation of $C_5H_8^+$—CH^+—CH_3 (C5-Min_1) into doublet C_5H_7═CH_2 and CH_3^{2+} species requires more than 370 kcal/mol at the B3LYP/cc-pVDZ level. The latter dication is a loosely bound species of C_{2v} symmetry that is characterized at the same theoretical level by C—H bond lengths (bond orders) equal to 1.65 Å (0.50) and 1.16 Å (1.02). This species is thus obviously prone to a straightforward dissociation into CH_2^+ and H^+. Indeed, at the B3LYP/cc-pVDZ level, the reaction energy and energy barrier for this process amount to −100.63 and +0.88 kcal/mol, respectively.

Similarly, dissociation of the $C_5H_8^+$—CH^+—CH_3 (C5-Min_1) intermediate into doublet $[C_5H_7$═$CH_2]^{2+}$ and CH_3 species is also highly unfavorable, in light of an endothermic reaction energy of more than 85 kcal/mol. Note also that, according to our calculations, further fragmentations through deprotonation of the $C_5H_7^+$═CH_2 species are energetically not at all favorable as these would require more than ~100 kcal/mol (~4 eV). Deprotonation of other dicationic species requires similar energies.[14]

Considering the energies that are involved in ionization processes, particularly for (e, 2e) experiments employing electron momentum spectroscopy and a kinetic energy of ~1.2 keV for the impinging electron, it is clear that, on long enough time scales, as with any experiments employing mass spectroscopy, the $C_5H_7^+$═CH_2 species will further decay through bond breaking and fragmentation. Because these processes require considerable energies (100 kcal/mol or more), their time scales certainly go beyond those encountered with electron- or photon-impact ionization spectroscopies such as EMS or UPS. In other words, these pathways go beyond the scope of our article.

C. Relaxation of Doubly Ionized Norbornane to a Six-Membered Monocyclic Species (C6-Min_4). Starting again from the S_2 (C_{2v}) structure of Figure 4a, the higher-lying third-order saddle point S_3 (C_s) could be obtained (Table 2, Figure 8) by lengthening the C_1—C_2 bond and letting the structure relax under the constraint of the C_s symmetry point group. Further distorting the S_3 (C_s) structure along the antisymmetric mode (Figure 8c) associated with the imaginary frequency 253i cm^{-1} and letting the structure relax without symmetry constraints yielded a structure that resembles the C5-Min_1 structure displayed in Figure 4d, with the only difference that the end CH^+—CH_3 group has undergone a rotation by ~180° about the C_3—C_6 bond. The obtained structure lies ~0.21 kcal/mol above C5-Min_1 and, except for a minor conformational rearrangement, is thus almost equivalent to the most stable structure for the identified five-membered cyclic species (C5-Min_x, $x = 1-3$). In contrast, distorting the above-mentioned S_3 (C_s) structure along the symmetric vibrational modes associated with the other two vibrational modes (Figure 8a,b) characterized by imaginary frequencies of 268i and 658i cm^{-1} results in the breaking of the C_2—C_1—C_3 bridge. In both cases, this induces an intramolecular rearrangement into the six-membered monocyclic dicationic species displayed in Figure 9. This species can be described as a 1,4-didehydrocyclohexane dicationic ring bearing a methyl substituent attached to one of the carbocationic centers. Very interestingly, this structure, referred to as C6-Min_4 (C_s) in Table 2, is located 11.87 kcal/mol *below* C5-Min_1. The two carbenium atoms (C_2 and C_3) are both located in the six-membered ring and exhibit a relatively larger intervening distance (2.92 Å) than in the C5-Min_1 species (3.74 Å). The increase in electrostatic repulsion between the charge centers is thus compensated here by more favorable inductive effects in a structure that contains one tertiary and one secondary

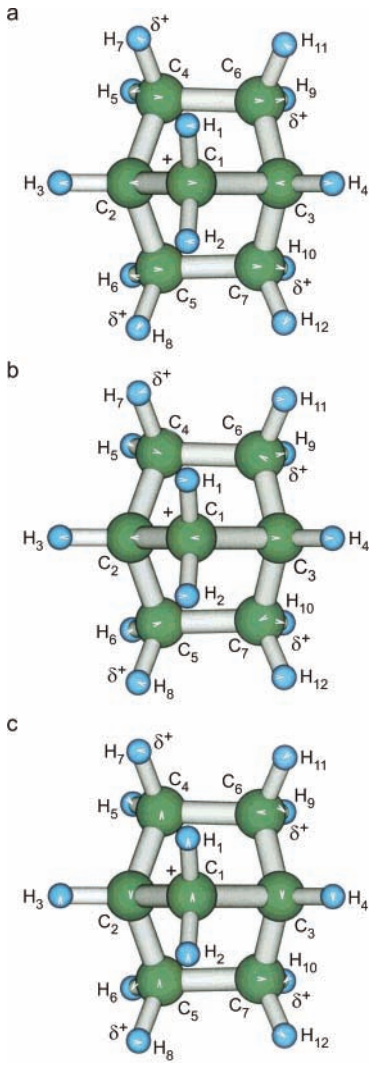

Figure 8. Structure of the third-order saddle point S_3 (C_s), along with the atomic displacements defining the three vibrational modes characterized by imaginary frequencies of (a) 658i, (b) 268i, and (c) 253i cm^{-1} at the B3LYP/cc-pVDZ level. The δ^+ and + symbols indicate moderate and strong localization of the charges created by double ionization, in line with the values reported in bold in Tables 3 and 4.

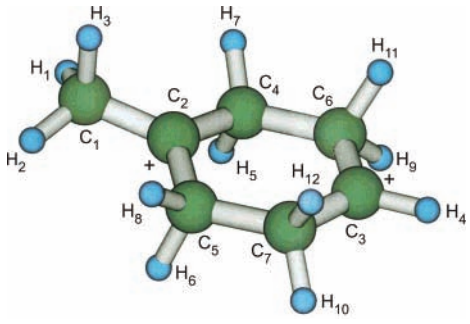

Figure 9. B3LYP/cc-pVDZ molecular structure of the C6-Min_4 (C_s) species. The δ^+ and + symbols indicate moderate and strong localization of the charges created by double ionization, in line with the values reported in bold in Tables 3 and 4.

carbocation. Here also, hyperconjugation between the empty C_{2p} orbital on C_2 and the adjacent C_1—H_3 bond should favorably stabilize this new dicationic structure. Deprotonation of the methyl tail of this structure was considered but found to be energetically not at all favorable ($\Delta E = +105.7$ kcal/mol). Also, attempts to find other minima by enforcing a proton transfer from C_1 to C_2 failed. We believe, therefore, that this structure can be merely regarded as a dead end in our search for suitable routes for an immediate charge fragmentation of norbornane^{2+} in its singlet ground state.

2. Focal-Point and Thermochemical Analyses of the Potential Energy Surface of Norbornane^{2+}. The B3LYP/cc-pVDZ results that have been discussed so far are supplemented in Table 2 by the results of calculations performed using the MPW1K functional and benchmark energy differences derived from a focal-point analysis (FPA) of estimates obtained by means of correlation treatments and basis sets of improving quality (Table 5). As can be seen in Table 2, most conclusions that have been drawn so far from calculations at a rather qualitative level resist a more robust and quantitative analysis. Considering the height of the computed barriers, B3LYP/cc-pVDZ energy differences and the results of single-point MPW1K/cc-pVDZ//B3LYP/cc-pVDZ energy calculations were found to be overall in good agreement, within relative accuracies on the order of 10%. The B3LYP values tend, in general, to underestimate the MPW1K values by 5−10 kcal/mol, which is consistent with former studies of intramolecular rearrangements using these functionals.[82−86,91,92] Reoptimizing the structures of the identified transition states at the MPW1K/cc-pVDZ level was also generally found to have only minor effects on the computed energy differences. All transition states and minima are, in general, correspondingly very comparable to the B3LYP/cc-pVDZ results, in view of both the structure and the computed bond orders and charge distributions. One exception arises with the S_1 (C_s) transition state, the structure of which was found to be extremely sensitive to the employed functional. It is a 1,5-didehydrocyclopentane dicationic ring bearing an ethyl substituent in the γ position relative to the first carbocationic center with, counterintuitively, partial positive charges that are located quite close to each other on the C_6 and C_7 atoms. Another difference arises with the C5-Min_3 structure, which corresponds to a rather shallow and high-lying energy minimum on the B3LYP/cc-pVDZ potential energy surface. This energy minimum, as well as the related transition states for proton transfers, could not be identified at the MPW1K/cc-pVDZ level, which presumably reflects the importance of through-space nonbonding interactions in this structure, which the MPW1K functional can underestimate as a result of the high proportion of Hartree−Fock exchange. All in all and in contrast to earlier works employing comparatively these two functionals, it appears that, regardless of the geometry, the B3LYP/cc-pVDZ results are most generally closer to results obtained at the CCSD(T)/cc-pVDZ level or from a benchmark focal-point analysis (FPA). This justifies a postiori the use of the B3LYP/cc-pVDZ approach for computing the potential energy surface of norbornane^{2+}.

We now examine in detail the determination of the energies of all identified stationary points relative to the C5-Min_1 structure within the confines of nonrelativistic quantum mechanics, i.e., via the FPA procedure. The values reported in Table 5 as ΔHF entries correspond to energy differences at the HF level, whereas the values reported as +MP2, +MP3, +CCSD, and +CCSD(T) entries are the corrections to these differences obtained by successively comparing the MP2 to the HF results; the MP3 to the MP2 results; the CCSD to the MP3 results; and finally, the CCSD(T) to the CCSD results. In each column, the sum of the reported values up to a given row associated with a specific theoretical model thus gives the relative energy for that particular model chemistry.

As a main example, we consider the evaluation of the energy of the S_2 (C_{2v}) species relative to the C5-Min_1 reference. From

TABLE 5: Focal-Point Analysis of the Energies (in kcal mol^{-1}) of the Identified Structures Relative to the $C_5H_8^+$−CH^+−CH_3 Intermediate[a]

		basis set (size[b])						basis set (size[b])			
		cc-pVDZ (158)	cc-pVTZ (378)	cc-pVQZ (745)	cc-pV∞Z			cc-pVDZ (158)	cc-pVTZ (378)	cc-pVQZ (745)	cc-pV∞Z
S_2 (C_{2v})	ΔHF	103.14	102.58	102.61	102.68[c]	TS_2^{PT}	ΔHF	21.41	20.84	20.81	20.85[c]
−C5-Min_1	+MP2	−61.87	−64.18	−64.44	−64.59[d]	−C5-Min_1	+MP2	−10.77	−11.25	−11.22	−11.27[d]
	+MP3	21.49	23.29				+MP3	2.89	3.22		
	+MP4[e]	2.78					+MP4[e]	0.37			
	+CCSD	0.40					+CCSD	0.27			
	+CCSD(T)	−8.85					+CCSD(T)	−0.88			
	total	57.09	56.02	55.79	55.71		total	13.29	12.57	12.57	12.56
S_1' (C_s)	ΔHF	49.50	47.62	47.32	47.28[c]	TS_3^{PT}	ΔHF	16.00	15.96	15.98	16.00[c]
−C5-Min_1	+MP2	−2.86	−2.74	−2.58	−2.58[d]	−C5-Min_1	+MP2	0.99	1.18	1.33	1.35[d]
	+MP3	1.15	1.42				+MP3	0.18	0.28		
	+MP4[e]	−0.51					+MP4[e]	−0.41			
	+CCSD	−0.06					+CCSD	−0.21			
	+CCSD(T)	−2.18					+CCSD(T)	−0.09			
	total	45.04	43.55	43.41	43.37		total	16.46	16.71	16.88	16.92
S_1 (C_s)	ΔHF	76.38	75.68	75.64	75.68[c]	TS^{Dis}	ΔHF	32.45	31.71	31.63	31.65[c]
−C5-Min_1	+MP2	−36.44	−38.15	−38.39	−38.51[d]	−C5-Min_1	+MP2	10.14	11.24	11.69	11.76[d]
	+MP3	10.82	11.65				+MP3	−1.34	−1.01		
	+MP4[e]	0.26					+MP4[e]	−0.95			
	+CCSD	0.97					+CCSD	−0.48			
	+CCSD(T)	−4.19					+CCSD(T)	0.74			
	total	47.80	46.22	45.94	45.86		total	40.56	41.25	41.62	41.71
C5-Min_2	ΔHF	6.78	6.51	6.49	6.51[c]	S_3 (C_s)	ΔHF	140.54	140.72	140.85	140.93[c]
−C5-Min_1	+MP2	−0.51	−0.73	−0.88	−0.94[d]	−C5-Min_1	+MP2	−54.86	−56.35	−56.41	−56.49[d]
	+MP3	0.07	0.09				+MP3	17.35	18.82		
	+MP4[e]	−0.10					+MP4[e]	0.28			
	+CCSD	0.04					+CCSD	−0.15			
	+CCSD(T)	−0.27					+CCSD(T)	−9.81			
	total	6.01	5.54	5.37	5.33		total	93.35	93.51	93.58	93.58
TS_1^{PT}	ΔHF	9.00	8.75	8.71	8.70[c]	C6-Min_4 (C_s)	ΔHF	−9.76	−9.83	−9.83	−9.83[c]
−C5-Min_1	+MP2	−4.55	−4.87	−4.96	−4.98[d]	−C5-Min_1	+MP2	0.26	−0.18	−0.39	−0.44[d]
	+MP3	0.89	1.07				+MP3	−0.28	−0.38		
	+MP4[e]	0.40					+MP4[e]	0.19			
	+CCSD	0.25					+CCSD	0.18			
	+CCSD(T)	−0.45					+CCSD(T)	0.12			
	total	5.54	5.15	5.02	4.99		total	−9.29	−9.90	−10.11	−10.16
C5-Min_3	ΔHF	15.95	14.37	14.33	14.45[c]	($C_5H_7^+$═CH_2	ΔHF	−17.81	−18.45	−18.51	−18.49[c]
−C5-Min_1	+MP2	−4.44	−5.22	−5.15	−5.28[d]	+ CH_3^+)	+MP2	10.57	11.68	12.17	12.25[d]
	+MP3	2.16	2.33			−C5-Min_1	+MP3	−1.31	−1.00		
	+MP4[e]	0.17					+MP4[e]	−0.91			
	+CCSD	0.12					+CCSD	−0.48			
	+CCSD(T)	−0.62					+CCSD(T)	0.86			
	total	13.34	11.15	11.18	11.17		total	−9.08	−8.30	−7.87	−7.77

[a] Calculations based on B3LYP/cc-pVDZ geometries. [b] Total number of atomic functions. [c] Results obtained using the extrapolation suggested by Feller.[78,79] [d] Results obtained using the extrapolation suggested by Schwartz.[81] [e] Fourth-order Møller-Plesset perturbation theory, using an excitation manifold comprising single, double, and quadruple electronic excitations.

Table 5, it is clear that, despite the importance of the corresponding energy difference in this case, the results obtained at the HF level converge extremely rapidly with basis sets of increasing size, and extrapolation to the limit of an asymptotically complete basis set within an accuracy of ∼0.05 kcal/mol is therefore straightforward. Corrections for electronic correlation at the second-order level and, to a lesser extent, at the third-order level of Møller−Plesset perturbation theory were found to be large and to converge more slowly to basis set completeness. Nonetheless, a comparison of the results obtained using the cc-pVTZ and cc-pVQZ basis sets as well as with the asymptotically complete cc-pV∞Z basis set (according to Schwartz's extrapolation procedure described in section II) indicates convergence of the MP2 energy differences within ∼0.2 kcal/mol. Because the absolute values of the successive correlation corrections tend to strongly decrease with the order attained in perturbation theory, it can be reasonably assumed that the +MP3/cc-pVTZ, +MP4SDQ/cc-pVDZ, +CCSD/cc-pVDZ, and +CCSD(T)/cc-pVDZ corrections represent optimal estimates of results that would be obtained using larger basis sets. Despite the oscillatory behavior of these corrections, this allows a determination of the S_2 (C_{2v})−C5-Min_1 (C_1) energy difference at the CCSD(T)/cc-pV∞Z level as follows : 102.68 − 64.59 + 23.29 + 2.78 + 0.40 − 8.85 = 55.71 kcal/mol. Note, nonetheless, that triple excitations have a rather substantial influence on the final results in this case, which is rather typical of a strongly stretched structure that is thus subject to significant electron correlation effects. Note also that, in general, the successive correlation corrections tend to scale proportionally to the computed energy differences and that the influence of triple excitations is comparatively much more limited for energy minima, as it should be.

For the sake of completeness, a thermochemical refinement of the potential energy surface is at last provided in Table 6. In

TABLE 6: Thermochemical Analysis of the Intramolecular Rearrangement and Fragmentation Processes Induced by Double Ionization of Norbornane, Including Differences in Electronic Energies (ΔE); Zero-Point Vibrational Energies (ΔZPVE); Enthalpies at 0 K (ΔH_0); and Enthalpies, Entropies, and Gibbs Free Energies at 298.15 K and 1 atm (ΔH_{298}, ΔS_{298} and ΔG_{298}, Respectively) Relative to the Kinetically Metastable C5-Min$_1$ Intermediate[a]

structure	ΔE[b]	freq	ΔZPVE	ΔH_0	ΔH_{298}	ΔS_{298}^{trans}	ΔS_{298}^{vib}	ΔS_{298}^{rot}	ΔS_{298}^{elec}	ΔS_{298}^{tot}	ΔG_{298}
S_1' (C_s)	43.37	232i	−1.26	42.11	42.12	0.000	0.451	−0.106	0.000	0.346	42.01
S_1 (C_s)	45.86	296i	0.55	46.41	45.36	0.000	−7.357	−0.960	0.000	−8.316	47.84
C5-Min$_1$	0.00	−	0.00	0.00	0.00	0.000	0.000	0.000	0.000	0.000	0.00
C5-Min$_2$	5.33	−	−0.91	4.42	4.57	0.000	1.279	0.001	0.000	1.280	4.19
TS$_1^{PT}$	4.99	483i	−1.18	3.81	3.55	0.000	−1.888	0.004	0.000	−1.884	4.11
C5-Min$_3$	11.17	−	1.65	12.82	12.61	0.000	−0.969	−0.222	0.000	−1.191	12.97
TS$_2^{PT}$	12.56	234i	0.70	13.26	12.57	0.000	−4.388	−0.272	0.000	−4.660	13.96
TS$_3^{PT}$	16.92	243i	0.44	17.36	17.06	0.000	−1.399	−0.036	0.000	−1.434	17.49
TS^{Dis}	41.71	91i	−3.14	38.57	39.69	0.000	12.076	1.141	0.000	13.217	35.75
C6-Min$_4$ (C_s)	−10.16	−	0.35	−9.81	−9.80	0.000	1.987	−0.099	0.000	1.888	−10.37
$C_5H_7^+$═CH_2 + CH_3^+	−7.77	−	−3.56	−11.33	−10.20[c]	33.562	−8.165	12.739	0.000	38.135	−21.57[c]

[a] Energies (enthalpies) and entropies given in kcal mol^{-1} and cal mol^{-1} K^{-1}, respectively. Imaginary frequencies (in cm^{-1}) characterizing the first-order saddle points (freq) are also listed. [b] Differences in total internal energies (ΔE) were derived from focal-point analyses (see Table 6); other thermochemical data were obtained by adding the B3LYP/cc-pVDZ estimates for zero-point vibrational energies to the ΔE values ($\Delta H_0 = \Delta E + \Delta$ZPVE), thermal corrections to the entropies ($\Delta H_{298} = \Delta H_0 + \Delta\Delta H_{298}$, with $\Delta\Delta H_{298} = \Delta H_{298} - \Delta H_{298}$ at the B3LYP/cc-pVDZ level), and entropy corrections to Gibbs free energies ($\Delta G_{298} = \Delta H_{298} - T\Delta S_{298}^{tot}$). [c] Mechanical work against external pressure ($RT = 0.59$ kcal/mol) included, assuming ideal-gas behavior.

this table, enthalpy differences at 0 K were calculated by adding (unrescaled) B3LYP/cc-pVDZ zero-point vibrational energies to the benchmark FPA estimates. Enthalpy differences at room temperature were evaluated by adding further thermal corrections derived from statistical thermodynamic partition functions calculated at the same level for energy minima and transition states using the RRHO approximation. The contribution from mechanical work (RT) against external pressure was taken into account in the evaluation of the reaction enthalpy for the dissociation of the $C_5H_8^+$—CH^+—CH_3 intermediate (the C5-Min$_1$ reference) into $C_5H_7^+$═CH_2 and CH_3^+. These data are supplemented by entropy differences obtained from the same partition functions, which were, in turn, used to calculate Gibbs free energy differences. As can be seen, all zero-point, thermal enthalpy, and entropy corrections have a marginal influence on the energy barriers and reaction energies for intramolecular rearrangements and proton transfers. For instance, the C6-Min$_4$ (C_s) species is located 11.87 kcal/mol below the C5-Min$_1$ species at the B3LYP/cc-pVDZ level. This energy difference reduces to 10.16 kcal/mol according to the focal-point analysis, yielding, in turn, a Gibbs free energy difference of 10.37 kcal/mol in favor of the C6-Min$_4$ species (Table 6).

In contrast, entropy effects were found to very substantially lower the reaction energy calculated for the dissociation of the $C_5H_8^+$—CH^+—CH_3 intermediate (the C5-Min$_1$ reference) into $C_5H_7^+$═CH_2 and CH_3^+, which is typical of radical dissociations.[88] Translations and rotations provide substantial positive contributions to the reaction enthalpy, whereas the vibrational contribution is negative and comparatively smaller in absolute value. These variations simply relate to the fact that, because of the cleavage of the $C_5H_8^+$—CH^+—CH_3 intermediate into smaller species, three additional rotational and three additional translation modes become available at the expense of six vibrational modes. Note that the rotational entropy of the $C_5H_7^+$═CH_2 species is only ∼1.37 cal mol^{-1} K^{-1} below that of the $C_5H_8^+$—CH^+—CH_3 intermediate; therefore, the increase in rotational entropy can be ascribed to the emission of a much smaller and rapidly spinning CH_3^+ moiety.

IV. Conclusions and Outlook for the Future

The main purpose of the present work was to identify at least one suitable pathway for a straightforward and ultrafast fragmentation of norbornane^{2+} into two distinct monocationic species, in an attempt to qualitatively explain an exceptionally intense and highly puzzling band at electron binding energies around the double-ionization threshold in the EMS ionization spectrum of the neutral species.[39,40] The potential surface of norbornane in its dicationic singlet ground state was therefore investigated in detail using density functional theory along with the nonlocal hybrid and gradient-corrected Becke three-parameter Lee−Yang−Parr functional (B3LYP) and the cc-pVDZ basis set. For the sake of more quantitative insight into these processes, this study was supplemented by a calculation of basic thermodynamic state functions coupled to a focal-point analysis of energy differences obtained using correlation treatments and basis sets of improving quality, enabling an extrapolation of these energy differences at the CCSD(T) level in the limit of an asymptotically complete (cc-pV∞Z) basis set.

Our best results indicate that geometric relaxation of the vertical doubly ionized state within the C_{2v} point group leads to a lowering of the molecular potential energy by 58.3 kcal/mol. An additional 55.7 kcal/mol can be converted into kinetic forms of energy by a bond breaking and straightforward rearrangement of the doubly charged norbornane cage into a five-membered cyclic $C_5H_8^+$—CH^+—CH_3 intermediate, with the ethyl cation substituent (CH^+—CH_3) in the γ position relative to the charge center in the five-membered cyclic ring. This process and the associated proton transfers were found to enable charge localization within different parts of the molecule. They are influenced by various competitive factors such as electrostatic interactions, inductive effects, cyclic strains, and methylenic hyperconjugation interactions. The above intermediate can be regarded as a kinetically metastable species, defining the entry gate to the dissociation pathway of norbornane^{2+} into $C_5H_7^+$═CH_2 and CH_3^+. Indeed, according to our best estimates, the corresponding reaction and activation enthalpies at 298 K and 1 atm amount to −10.2 and + 39.7 kcal/mol, respectively. The heterolytic charge fragmentation of the $C_5H_8^+$—CH^+—CH_3 singlet species into $C_5H_7^+$═CH_2 and CH_3^+ singlet species possibly involves a transient or short-lived $C_5H_7^{2+}$—CH_2—CH_3 species that is ∼3.3−5.3 kcal/mol above the $C_5H_8^+$—CH^+—CH_3 intermediate; this structure corresponds to a shallow energy minimum on the B3LYP/cc-pVDZ surface and possibly to an energy shoulder on the potential energy curve associated with

the fragmentation channel at a benchmark many-body quantum mechanical level [CCSD(T)/cc-pV∞Z]. In view of an estimated energy barrier of only 5.0−6.0 kcal/mol, this proton transfer will certainly be favored by pronounced tunneling effects[94] and can therefore be regarded as incommensurably faster than the charge fragmentation itself. Entropy effects were found to tremendously favor the charge fragmentation, through a contribution of −11.4 kcal mol^{-1} to the Gibbs free reaction energy at 298 K.

In our quest for additional straightforward pathways and clues for an ultrafast Coulomb fragmentation of norbornane^{2+}, an opening of the methylene bridge led us to identify a six-membered cyclic structure ($C_6H_9^{2+}$—CH_3) in the form of a 1,4-didehydrocyclohexane dicationic ring bearing a methyl substituent attached to one of the carbocationic centers, at an energy 10.2 kcal/mol below that of the $C_5H_8^+$—CH^+—CH_3 species, according to our best estimates. On the singlet ground-state potential energy surface of norbornane^{2+}, this structure can be regarded as a dead end on short time scales ($<10^{-9}$ s), because a charge fragmentation into distinct monocationic species would at least imply the breaking of two single C—C bonds.

Considering the energy released ($\Delta H_{298} = 114.0$ kcal/mol) by molecular relaxation of norbornane^{2+} after the sudden removal of two electrons from the neutral, compared to the energy barrier ($\Delta H^{\dagger}_{298} = 39.7$ kcal/mol) to overcome for a charge fragmentation of the $C_5H_8^+$—CH^+—CH_3 intermediate, it seems more than plausible that, at ionization energies around the double-ionization threshold and following a purely electronic and thus straightforward *intra*molecular Coulomb decay of shakeup states into dissociative shakeoff states, norbornane becomes subject to ultrafast nuclear dynamical processes involving intramolecular rearrangements and Coulomb explosion into monocationic species. Because a vertical double-ionization process leads to a second-order saddle point under relaxation within the C_{2v} point group, a breaking of the Born−Oppenheimer approximation is likely to occur, which is in line with the range of time scales (from $\sim10^{-15}$ to $\sim10^{-13}$ s) inferred previously[40] for these rearrangement processes from a comparison of UPS (He I) and EMS ($E_k = 1.5$ keV) measurements. Ultrafast nuclear dynamics would then explain the unusually large width of the bands observed at electron binding energies above ~25 eV,[39] indicating considerable natural broadening due to very limited lifetimes. Ultrafast nuclear dynamics might also be related to the unusually large (e, 2e) ionization intensities recorded under EMS conditions at these electron binding energies. An argument in favor of this fairly daring hypothesis is a very severe upturn[95] of the (e, 2e) ionization intensity associated with the fully dissociative $^2\Sigma_u(2p\sigma_u)$ shakeup state of H_2, which so far still eludes all theoretical explanations, even upon considering advanced (second-order Born) treatments of distorted wave effects.[96] It is thus worth recalling that the interaction operator governing transition amplitudes in (e, 2e) ionization processes explicitly depends on the electronic *and nuclear* coordinates.[97] We thus suspect that the final answer to the band 12 issue in the EMS ionization spectrum of norbornane might be strongly related to the dissociative nature of the potential energy surface that has been computed for the dicationic ground state of this compound.

To be fully reliable, a complete interpretation of EMS experiments on norbornane throughout the valence region of norbornane should therefore consistently cover the four spaces underlying quantum mechanics, namely, the energy, time, configuration, and momentum spaces. In our work, we simply studied, within the framework of the Born−Oppenheimer approximation, the structural consequences of a double-ionization event resulting from the sudden removal of two electrons, assuming that no residual nuclear kinetic energy remained in the initial state. In other words, we considered as initial state the shakeoff state that lies precisely at an electron binding energy equal to the vertical double-ionization energy of norbornane (~26.5 eV according to our best data). Note that the initial state in the geometric process lies high above the energy barrier leading to dissociation of the cage into smaller fragments and is thus not subject to a quantization of the vibrational and rotational energies over stationary states. On the contrary, vibrational and rotational motions for the states above the double-ionization threshold that would be generated using high-energy photons are by definition of transient nature, as these states are embedded in an energy continuum. Further studies employing nuclear dynamics[98] or wave packet dynamics[99] around conical intersections[100] will probably be necessary for a quantitative evaluation of the effects of vibrational and rotational excitations on the dynamics that can be predicted from the computed potential energy landscape and for an investigation of the influence of the identified intramolecular rearrangement and charge dissociation processes on the innermost valence ionization spectrum of norbornane, as well as on the corresponding electron distributions in the configuration and momentum spaces.

Acknowledgment. This work was supported by the Bijzonder OnderzoeksFonds (BOF) of Hasselt University and the Fonds voor Wetenschappelijk Onderzoek-Vlaanderen (FWO, the Flemish branch of the National Scientific Foundation of Belgium). B.H. is postdoctoral researcher at Hasselt University and acknowledges financial support from the research community "Quantum Chemistry: Applied and Fundamental Aspects of Density Functional Theory". The authors thank Dr. P. De Maesschalck for his kind help in preparing Figure 3. Mrs. Y. R. Huang is acknowledged for useful discussions.

Supporting Information Available: Detailed Cartesian coordinates and energies for all structures displayed in Figures 4, 5, 6, 8, and 9 are available free of charge via the Internet at http://pubs.acs.org.

References and Notes

(1) Shields, G. C.; Moran, T. P. *Theor. Chim. Acta* **1986**, *69*, 147.
(2) Lammertsma, K.; von Schleyer, R. P.; Schwarz, H. *Ang. Chem., Int. Ed. Engl.* **1989**, *28*, 1321.
(3) Mathur, D. *Phys. Rep.* **1993**, *225*, 193.
(4) See the special issue on multiply charged ions: *Int. J. Mass. Spectrom.* **1999**, *192*.
(5) Schröder, D.; Schwarz, H. *J. Phys. Chem. A* **1999**, *103*, 7385.
(6) Nenajdenko, V. C.; Shevchenko, N. E.; Balenkova, E. S.; Alabugin, I. V. *Chem. Rev.* **2003**, *103*, 229.
(7) Mathur, D. *Phys. Rep.* **2004**, *391*, 1.
(8) Basch, H.; Hoz, S.; Goldberg, M. *Isr. J. Chem.* **1993**, *33*, 403.
(9) Hensen, K.; Stumpf, T.; Bolte, M.; Nätscher, C.; Fleischer, H. *J. Am. Chem. Soc.* **1998**, *120*, 10402.
(10) Tafadar, N.; Kaltsoyanis, N.; Price, S. D. *Int. J. Mass. Spectrom.* **1999**, *192*, 205.
(11) Kroto, H. W.; Heath, J. R.; O' Brion, S. C.; Curl, R. F.; Smalley, R. E. *Nature* **1985**, *318*, 162.
(12) Cioslowski, J.; Patchovski, S.; Thiel, W. *Chem. Phys. Lett.* **1996**, *248*, 116.
(13) (a) Scheier, P.; Märk, T. D. *Phys. Rev. Lett.* **1994**, *73*, 54. (b) Jin, J.; Khemliche, H.; Prior, M. H.; Xie, Z. *Phys. Rev. A* **1996**, *53*, 615.
(14) Deleuze, M. S.; François, J.-P.; Kryachko, E. *J. Am. Chem. Soc.* **2005**, *127*, 16824.
(15) Nicolaides, C. A. *Chem. Phys. Lett.* **1989**, *161*, 547.

(16) (a) Benoit, C.; Horsley, J. A. *Mol. Phys.* **1975**, *30*, 557. (b) Lammertsma, K.; Barzaghi, M.; Olah, G. A.; Pople, J. A.; Kos, A. J.; von Schleyer, R. P. *J. Am. Chem. Soc.* **1983**, *105*, 5252.

(17) Maier, G. *Angew. Chem.* **1988**, *100*, 317.

(18) Carnadi, H.; Giordano, C.; Heldeweg, R. F.; Hogeveen, H.; E. M. G. A. van Kruchten *Isr. J. Chem.* **1981**, *21*, 229.

(19) Prakash, G. K. S.; Krishnamurthy, V. V.; Herges, R.; Bau, R.; Yuan, H.; Olah, G. A. *J. Am. Chem. Soc.* **1986**, *108*, 836. (b) Prakash, G. K. S.; Krishnamurthy, V. V.; Herges, R.; Bau, R.; Yuan, H.; Olah, G. A.; Fessner, W. D.; Prinzbach, J. *J. Am. Chem. Soc.* **1988**, *110*, 7764. (c) Weber, K.; Lutz, G.; Knothe, L.; Mortensen, J.; Heinze, J.; Prinzbach, H. *J. Chem. Soc., Perkin Trans. 2* **1995**, 1991.

(20) (a) Bremer, M.; Schleyer, P. v. R.; Schoetz, K.; Kausch, M.; Schindler, M. *Angew. Chem., Int. Ed. Engl.* **1987**, *26*, 761. (b) Fokin, A. A.; Kiran, B.; Bremer, M.; Yuang, X. M.; Jiao, H. J.; Schreiner, P. R. *Chem. Eur. J.* **2000**, *6*, 1615.

(21) Price, S. D.; Manning, M.; Leone, S. R. *J. Am. Chem. Soc.* **1994**, *116*, 8673.

(22) Price, S. D. *Phys. Chem. Chem. Phys.* **2003**, *5*, 1717.

(23) Roithová, J.; Herman, Z.; Schröder, D.; Schwarz, H. *Chem.-Eur. J.* **2006**, *12*, 2465.

(24) Roithová, J.; Schröder, D.; Schwarz, H. *J. Phys. Chem. A* **2004**, *108*, 5060.

(25) Roithová, J.; Schröder, D.; Schwarz, H. *Chem.-Eur. J.* **2005**, *11*, 627.

(26) Roithová, J.; Schröder, D.; Loos, J.; Schwarz, H.; Jankowiak, H.-Ch.; Berger, R.; Thissen, R.; Dutuit, O. *J. Chem. Phys.* **2005**, *122*, 094306.

(27) Leach, S. W. *Z. Phys. Chem.* **1996**, *195*, 15.

(28) Buchbauer, G.; Pauzenberger, I. *Pharmazie* **1999**, *54*, 5.

(29) Chiang, J. F.; Wilcox, C. F.; Bauer, S. H. *J. Am. Chem. Soc.* **1968**, *90*, 3149.

(30) Choplin, A. *Chem. Phys. Lett.* **1980**, *71*, 503.

(31) Bischof, P.; Hashmall, J. A.; Heilbronner, E; Hornung, V *Helv. Chim. Acta* **1969**, *52*, 1745.

(32) Getzlaff, M.; Schönhense, G. *J. Electron Spectrosc. Relat. Phenom.* **1998**, *95*, 225.

(33) Bieri, G.; Burger, F.; Heilbronner, E.; Maier, J. P. *Helv. Chim. Acta* **1977**, *60*, 2213.

(34) Weigold, E.; McCarthy, I. E. *Electron Momentum Spectroscopy*; Kluwer Academic/Plenum Publishers: New York, 1999.

(35) Schirmer, J.; Cederbaum, L. S.; Walter, O. *Phys Rev A* **1983**, *28*, 1237.

(36) Schirmer, J.; Angonoa, G. *J. Chem. Phys.* **1989**, *91*, 1754.

(37) Weikert, H. G.; Meyer, H.-D.; Cederbaum, L. S.; Tarantelli, F. *J. Chem. Phys.* **1996**, *104*, 7122.

(38) Deleuze, M. S.; Giuffreda, M. G.; François, J.-P.; Cederbaum, L. S. *J. Chem. Phys.* **1999**, *111*, 5851.

(39) Knippenberg, S.; Nixon, K. L.; Brunger, M. J.; Maddern, T.; Campbell, L.; Trout, N.; Wang, F.; Newell, W. R.; Deleuze, M. S.; François, J.-P.; Winkler, D. A. *J. Chem. Phys.* **2004**, *121*, 10525.

(40) Knippenberg, S.; Deleuze, M. S.; Cleij, T. J.; François, J.-P.; Cederbaum, L. S.; Eland, J. H. D. *J. Phys. Chem. A* **2005**, *109*, 4267.

(41) Cederbaum, L. S.; Zobeley, J.; Tarantelli, F. *Phys. Rev. Lett.* **1997**, *79*, 4778.

(42) Marburger, S.; Kugeler, O.; Hergenhahn, U.; Möller, T. *Phys. Rev. Lett.* **2003**, *90*, 203401.

(43) Jahnke, T.; Czasch, A.; Schöffler, M. S.; Schössler, S.; Knapp, A.; Käsz, M.; Titze, J.; Wimmer, C.; Kreidi, K.; Grisenti, R. E.; Staudte, A.; Jagutzki, O.; Hergenhahn, U.; Schmidt-Böcking, H.; Dörner, R. *Phys. Rev. Lett.* **2004**, *93*, 163401.

(44) Frisch, M. J.; Trucks, G. W.; Schlegel, H. B.; Scuseria, G. E.; Robb, M. A.; Cheeseman, J. R.; Zakrzewski, V. G.; Montgomery, J. A., Jr.; Stratmann, R. E.; Burant, J. C.; Dapprich, S.; Millam, J. M.; Daniels, A. D.; Kudin, K. N.; Strain, M. C.; Farkas, O.; Tomasi, J.; Barone, V.; Cossi, M.; Cammi, R.; Mennucci, B.; Pomelli, C.; Adamo, C.; Clifford, S.; Ochterski, J.; Petersson, G. A.; Ayala, P. Y.; Cui, Q.; Morokuma, K.; Malick, D. K.; Rabuck, A. D.; Raghavachari, K.; Foresman, J. B.; Cioslowski, J.; Ortiz, J. V.; Stefanov, B. B.; Liu, G.; Liashenko, A.; Piskorz, P.; Komaromi, I.; Gomberts, R.; Martin, R. L.; Fox, D. J.; Keith, T.; Al-Laham, M. A.; Peng, C. Y.; Nanayakkara, A.; Gonsalez, C.; Challacombe, M.; Gill, P. M. W.; Johnson, B. G.; Chen, W.; Wong, M. W.; Andres, J. L.; Head-Gordon, M.; Replogle, E. S.; Pople, J. A. *Gaussian 98*, revision A.7; Gaussian, Inc.: Pittsburgh, PA, 1998.

(45) (a) Lee, C.; Yang, W.; Parr, R. G. *Phys. Rev. B* **1988**, *37*, 785. (b) Becke, A. D. *J. Chem. Phys.* **1993**, *98*, 5648.

(46) Dunning, T. H., Jr. *J. Chem. Phys.* **1989**, *90*, 1007.

(47) Simons, J.; Jorgensen, P.; Taylor, H.; Ozment, J. *J. Phys. Chem.* **1983**, *87*, 2745.

(48) Peng, C.; Schlegel, H. B. *Isr. J. Chem.* **1994**, *33*, 449.

(49) Peng, C.; Ayala, P. Y.; Schlegel, H. B.; Frisch, M. J. *J. Comput. Chem.* **1996**, *17*, 49.

(50) Seeger, R.; Pople, J. A. *J. Chem. Phys.* **1977**, *66*, 3045.

(51) Bauernschmitt, R.; Ahlrichs, R. *J. Chem. Phys.* **1996**, *104*, 9047.

(52) Cizek, J. *Adv. Chem. Phys.* **1969**, *14*, 35.

(53) Purvis, G. D.; Bartlett, R. J. *J. Chem. Phys.* **1982**, *76*, 1910.

(54) Scuseria, G. E.; Janssen, C. L.; Schaefer, H. F., III. *J. Chem. Phys.* **1988**, *89*, 7382.

(55) Scuseria, G. E.; Schaefer, H. F., III. *J. Chem. Phys.* **1989**, *90*, 3700.

(56) Lee, T. J.; Taylor, P. R. *Int. J. Quantum Chem. Symp.* **1989**, *23*, 199.

(57) (a) Werner, H.-J.; Knowles, P. J.; Lindh, R.; Manby, F. R.; Schütz, M.; Celani, P.; Korona, T.; Rauhut, G.; Amos, R. D.; Bernhardsson, A.; Berning, A.; Cooper, D. L.; Deegan, M. J. O.; Dobbyn, A. J.; Eckert, F.; Hampel, C.; Hetzer, G.; Lloyd, A. W.; McNicholas, S. J.; Meyer, W.; Mura, M. E.; Nicklass, A.; Palmieri, P.; Pitzer, R.; Stoll, H.; Stone, A. J.; Tarroni, R.; Thorsteinsson, T. *MOLPRO*, version 2000.1; University College Cardiff Consultants Limited: Cardiff, U.K., 2000; see http://www.molpro.net. (b) Lindh, R.; Ryu, U.; Liu, B. *J. Chem. Phys.* **1991**, *95*, 5889. (c) Hampel, C.; Peterson, K.; Werner, H.-J. *Chem. Phys. Lett.* **1992**, *190*, 1.

(58) Roos, B. O.; Taylor, P. R.; Siegbahn, P. E. M. *Chem. Phys.* **1980**, *48*, 157.

(59) McQuarrie, D. A. *Statistical Mechanics*; University Science Books, Sausalito, CA, 2000.

(60) Glendening, E. D.; Reed, A. E.; Carpenter, J. E.; Weinhold, F *NBO*, version 3.1; Theoretical Chemistry Institute, University of Wisconsin: Madison, WI, 1993.

(61) Carpenter, J. E.; Weinhold, F. *J. Mol. Struct. (THEOCHEM)* **1988**, *169*, 41.

(62) Foster, J. P.; Weinhold, F. *J. Am. Chem. Soc.* **1980**, *102*, 7211.

(63) Reed, A. E.; Weinhold, F. *J. Chem. Phys.* **1983**, *78*, 4066.

(64) Reed, A. E.; Weinhold, F. *J. Chem. Phys.* **1983**, *78*, 1736.

(65) Reed, A. E.; Weinstock, R. B.; Weinhold, F. *J. Chem. Phys.* **1985**, *83*, 735.

(66) Reed, A. E.; Curtiss, L. A.; Weinhold, F. *Chem. Rev.* **1988**, *88*, 899.

(67) Weinhold, F.; Carpenter, J. E. In *The Structure of Small Molecules and Ions*; Naaman, R., Vager, Z., Eds.; Plenum Press: New York, 1988; pp 227−236.

(68) Szabo, A.; Ostlund, N. S. *Modern Quantum Chemistry: Introduction to Advanced Electronic Structure Theory*; Dover Publications Inc.: New York, 1996.

(69) Møller, C.; Plesset, M. S. *Phys. Rev.* **1934**, *46*, 618.

(70) Binkley, J. S.; Pople, J. A. *Int. J. Quantum Chem.* **1975**, *9*, 229.

(71) Pople, J. A.; Binkley, J. S.; Seeger, R. *Int. J. Quantum Chem. Symp.* **1976**, *10*, 1.

(72) Krishnan, R.; Pople, J. A. *Int. J. Quantum Chem.* **1978**, *14*, 91.

(73) Pople, J. A.; Head-Gordon, M.; Raghavachari, K. *J. Chem. Phys.* **1987**, *87*, 5968.

(74) Allinger, N. L.; Fermann, J. T.; Allen, W. D.; Schaefer, H. F., III. *J. Chem. Phys.* **1997**, *106*, 5143.

(75) Salam, A.; Deleuze, M. S. *J. Chem. Phys.* **2002**, *116*, 1296.

(76) Kwasniewski, S. P.; Claes, L.; François, J.-P.; Deleuze, M. S. *J. Chem. Phys.* **2003**, *118*, 7823.

(77) Huang, Y. R.; Knippenberg, S.; Hajgato, B.; François, J.-P.; Deng, J. K.; Deleuze, M. S. *J. Phys. Chem. A* **2007**, *111*, 5879.

(78) Feller, D. *J. Chem. Phys.* **1992**, *96*, 6104.

(79) Feller, D. *J. Chem. Phys.* **1993**, *98*, 7059.

(80) Martin, J. M. L. *Ab Initio Thermochemistry Beyond Chemical Accuracy for First- and Second-Row Compounds*. In *Energetics of Stable Molecules and Reactive Intermediates*; NATO ASI Symposium Volume ASIC 535; Minas da Piedade, M. E., Irikura, K. K, Eds.; Kluwer Academic Publishers: Dordrecht, The Netherlands, 1999.

(81) Schwartz, C. In *Methods in Computational Physics 2*; Alder, B. J., Fernbach, S., Rotenberg, M., Eds.; Academic Press: New York, 1963; p 241.

(82) Lynch, B. J.; Truhlar, D. G. *J. Phys. Chem. A* **2001**, *105*, 2936.

(83) Deleuze, M. S.; Claes, L.; Kryachko, E. S.; François, J.-P. *J. Chem. Phys.* **2003**, *106*, 8569.

(84) Zhao, Y.; Truhlar, D. G. *J. Phys. Chem. A* **2004**, *108*, 6908.

(85) Zhao, Y.; Lynch, B. J.; Truhlar, D. G. *J. Phys. Chem. A* **2004**, *108*, 4786.

(86) Zhao, Y.; Pu, J.; Lynch, B. J.; Truhlar, D. G. *Phys. Chem. Chem. Phys.* **2004**, *6*, 673.

(87) Lynch, B. J.; Fast, P. L.; Harris, M.; Truhlar, D. G.; *J. Phys. Chem. A* **2000**, *104*, 4811.

(88) Claes, L.; François, J.-P.; Deleuze, M. S. *J. Am. Chem. Soc.* **2003**, *125*, 7129.

(89) Claes, L.; François, J.-P.; Deleuze, M. S. *J. Comput. Chem.* **2003**, *24*, 2023.

(90) Wiberg, K. *Tetrahedron* **1968**, *24*, 1083.

(91) McMurry, J. *Organic Chemistry*; Brooks/Cole: Belmont, CA, 2004.

(92) Deleuze, M.; Denis, J.-P.; Delhalle, J.; Pickup, B. T. *J. Phys. Chem.* **1993**, *97*, 5115.

(93) Gilbert, R. G.; Smith, S. C. *Theory of Unimolecular and Recombination Reactions*; Blackwell Scientific Publications: Oxford, U.K., 1990.
(94) Cukier, R. I. *J. Phys. Chem.* **1995**, *99*, 16101.
(95) Takahashi, M.; Khajuria, Y.; Udagawa, Y. *Phys. Rev. A* **2003**, *68*, 042710; (b) Takahashi, M. M.; Watanabe, N.; Khajuria, Y.; Nakayama, K.; Udagawa, Y.; Eland, J. H. D. *J. Electron Spectrosc. Relat. Phenom.* **2004**, *141*, 83.
(96) Dal Capello, C.; Mansouri, A.; Houamer, L. S.; Joulakian, B. *J. Phys. B* **2006**, *39*, 2431.
(97) See a paper presented at the International Conference on Electron and Photon Impact Ionization and Related Topics, Louvain-la-Neuve, Belgium, 2004: Stia, C. R.; Fojon, O. A.; Rivarola, R. D.; Hanssen, J.; Kamalou, O.; Martina, D.; Chesnel, J.-Y.; Frémont, F. *Inst. Phys. Conf. Ser.* **2005**, *183*, 73.
(98) See: Köppel, H. In *Quantum Dynamics of Complex Molecular Systems*; Micha, D. A., Burghardt, I., Eds.; Springer: Heidelberg, 2006; see also references therein.
(99) See: Manz, J.; Wöste, L. *Femtosecond Chemistry*; Verlag Chemie: Weinheim, Germany, 1995; see also references therein.
(100) See: Domcke, W.; Yarkony, D. R.; Köppel, H. *Conical Intersections: Electronic Structure, Dynamics and Spectroscopy*; World Scientific: Singapore, 2004; see also references therein.